UCRL-1767
Unclassified-Physics Distribution

UNIVERSITY OF CALIFORNIA

Radiation Laboratory

Contract No. W-7405-eng-48

UNCLASSIFIED

DISINTEGRATION OF HELIUM BY 90 MEV NEUTRONS

Peter E. Tannenwald

(Thesis)

April, 1952

Berkeley, California

DISCLAIMER

This document was prepared as an account of work sponsored by the United States Government. While this document is believed to contain correct information, neither the United States Government nor any agency thereof, nor the Regents of the University of California, nor any of their employees, makes any warranty, express or implied, or assumes any legal responsibility for the accuracy, completeness, or usefulness of any information, apparatus, product, or process disclosed, or represents that its use would not infringe privately owned rights. Reference herein to any specific commercial product, process, or service by its trade name, trademark, manufacturer, or otherwise, does not necessarily constitute or imply its endorsement, recommendation, or favoring by the United States Government or any agency thereof, or the Regents of the University of California. The views and opinions of authors expressed herein do not necessarily state or reflect those of the United States Government or any agency thereof or the Regents of the University of California.

TABLE OF CONTENTS

page

ABSTRACT 4

I. INTRODUCTION 6

II. EXPERIMENTAL PROCEDURE 7

1. Apparatus 7

2. Operation 8

3. Photography 9

III. METHOD OF ANALYSIS OF EVENTS 9

1. Available Data 10

2. Identification Procedure 10

3. Errors in Measurement 15

4. Calculations 16

IV. CORRECTIONS 19

1. Single-Prong Stars 19

2. Two-Prong Stars 20

3. The He^3 Assumption 22

V. RESULTS AND DISCUSSION 23

1. Inelastic Events 23

2. Elastic Events 27

3. Cross Sections 29

4. Errors 30

5. Comparison With Theory 31

6. Energy Dependence 32

7. Energy and Angular Distributions 34

8. Oxygen Stars 38

9. Azimuthal Symmetry Check 39

VI. CONCLUSIONS 40

VII. ACKNOWLEDGMENTS 41

APPENDIX I DEFINITIONS 59

APPENDIX II SAMPLE ANALYSIS OF TWO PICTURES 59

APPENDIX III DERIVATION OF FORMULAS 63

APPENDIX IV TABLE OF IONIZATIONS 65

REFERENCES 69

DISINTEGRATION OF HELIUM BY 90 MEV NEUTRONS

Peter E. Tannenwald

ABSTRACT

An experiment was undertaken to make a detailed study in a cloud chamber of the fragments produced from helium nuclei when bombarded by high energy neutrons. 90 Mev neutrons produced by stripping 190 Mev deuterons in the 184-inch cyclotron were collimated and sent through a 22-inch pantograph cloud chamber filled with helium gas to a total pressure of 81.5 cm Hg. The chamber was operated in a pulsed magnetic field of 21,700 gauss. The possible disintegration products are:

INELASTIC	triton and deuteron (dt)
	two deuterons and a neutron (dd)
	triton, proton and a neutron (pt)
	deuteron, proton and two neutrons (pd)
	two protons and three neutrons (pp)
	He^3 and two neutrons (He^3)
ELASTIC	He^4 and a neutron (He^4)

The particles from the two-prong stars were identified by curvature and relative ionization, and the single tracks by characteristic track endings (change of radius with residual range) when they ended in the chamber. For dt, dd, pt and He^4 events the energy of the incident neutrons could be calculated from the measured quantities (minimum only for pd events). A weighting factor was computed for each one- and two-prong star analyzed, which corrects for events which were too slanted to be measured. Since the number of He^3's

was uncertain because they could not be distinguished from He^4's when the track did not end in the chamber, the ratio of He^3/pt events was assumed to be the same as the ratio of σ_{nn}/σ_{np} at 90 Mev. The total number of events, for incident neutrons above 40 Mev, was normalized to the interpolated n - He^4 total cross section of 1.9×10^{-25} cm^2; thus absolute cross sections for the various disintegration processes could be established. Energy dependences and energy and angular distributions have also been determined.

DISINTEGRATION OF HELIUM BY 90 MEV NEUTRONS

Peter E. Tannenwald

I. INTRODUCTION

Scattering experiments are one of the fundamental ways of gaining information about nuclear forces. Nucleon-nucleon scattering evidently provides the most direct way of getting at the interactions between neutrons and protons. Yet the scattering and disintegration of nuclei by nucleons has been a most fruitful approach in establishing various models of the nucleus and in revealing the behavior of large numbers of nucleons in close proximity. The disintegration of helium presents a unique case in that there are few enough particles so that a theoretical analysis of the interactions between individual nucleons can be hoped for; and on the other hand, due to the tightly bound structure of helium it will show some of the properties of heavier nuclei. If it is true, as is sometimes believed, that the alpha particle exists as a sub-structure in heavier nuclei, then the disintegration of helium will certainly be of value in interpreting the disintegrations of heavier nuclei.

The charged particles ejected from nuclei when bombarded by 90 Mev neutrons have been studied[(1),(2)] in a number of experiments, and the results indicate that the nature of the collision process for high energies is determined predominantly by the interaction of the bombarding particle with an individual nucleon rather than with the struck nucleus as a whole. The general features, first outlined by Goldberger[(3)], include fast particles ejected in the forward direction and low energy particles emitted more or less isotropically. An unexpected result of these experiments was the

relatively large yield of the fast deuterons (and also tritons) in the forward direction. The production of these deuterons has been explained by Chew and Goldberger[4] in terms of a "pick-up" process, in which the incident neutron moves off with a proton when the latter has a momentum and position so as to constitute a deuteron with the incoming neutron.

It has become customary to denote the splitting up of a nucleus as a star when the event through one or more charged particles is visible in a cloud chamber or nuclear emulsion. Neutron-induced stars are especially suited for study with a cloud chamber. The first star experiment using 90 Mev neutrons was carried out by Tracy and Powell[5], who filled this chamber with a mixture of oxygen and helium gas. Analysis of the stars was a difficult task mainly because of the presence of oxygen nuclei. That a more complete analysis was possible in the present investigation may be ascribed largely to the use of helium gas alone in the chamber, a more powerful magnetic field[6], and experience with neutron-deuteron scattering[7].

II. EXPERIMENTAL PROCEDURE

1. Apparatus

The 90 Mev neutrons produced in the stripping process by bombarding a 2 inch thick beryllium target with 190 Mev deuterons were collimated outside the concrete shielding of the 184-inch Berkeley cyclotron by means of a rectangular copper collimator four feet long passing a beam 2 3/4 in. wide and 3/4 in. high. (See Figs. 1 and 2). The neutrons were then allowed to enter a 22 in. Wilson cloud chamber[6] through a 3 x 1 inch aluminum foil 1 mil thick, and to pass

out through a similar window in order to reduce back-scattering from the rear wall of the chamber. The bottom of the chamber consisted of a rubber-covered half-inch thick lucite disk which moved vertically, and was controlled by a pantagraph which kept it accurately horizontal during the expansions. The disk was covered with a black dye dissolved in gelatin in order to give a perfectly black background for the tracks. A General Electric FT422 flash tube was placed on each side of the chamber, whose illumination had previously been checked to be uniform over 2 1/2 in. in the 3 1/2 in. high chamber[7]. Each lamp was flashed by discharging 1024μf condensers charged to 1700 volts through it.

2. Operation

The cloud chamber was operated in a pulsed magnetic field of 22,000 gauss which was energized by a 150 h.p. mine-sweeper generator. The field in the magnet takes about 2.5 sec. to build up to its maximum value, where it remains steady for about 0.15 sec. before being turned off. The cycle of operations, which is repeated once a minute, is as follows: the current is turned on in advance so that its maximum coincides with the expansion of the chamber. The cyclotron beam is pulsed through the chamber at the instant the moving diaphragm hits the bottom, and the lights are flashed 0.03 sec. after this. The current which passes through the magnet is automatically recorded with each picture because the camera has a third lens which views the magnet current ammeter. The whole chamber is kept at a constant temperature of 19.3° C by means of a temperature-controlled circulating water system. A clearing field of about 400 volts is turned off just before the chamber starts to expand and is turned on again after the lights have flashed.

The chamber was filled with 99 percent pure helium gas to a total pressure of 81.5 cm Hg; in the expanded equilibrium position 1.8 cm of this pressure was due to the partial water vapor pressure from the gelatine. The chamber was then compressed to 20 cm above atmospheric pressure, forcing some water vapor molecules back into the gelatine, and resulting in helium to oxygen nuclei ratio of 51.8. This same ratio existed immediately after expansion because the water vapor had no chance to get into equilibrium. The expansion ratio during the experiment was around 17 percent.

3. Photography

A specially constructed stereoscopic camera was mounted on a light-tight dome 27 inches above the top-glass of the chamber. The pictures were taken through a pair of Leica lenses at f 5.6 and f 6.3 on Eastman Linograph Ortho film in 100 ft. strips 1.80 in. wide. Life-size reprojection on a translucent screen was made by means of a double projector which duplicated the geometry of the camera optical system and employed the camera lenses. Western Union arc lamps type 300 K provided brilliant projected images. Reference (8) describes the reprojection apparatus in more detail, and the sketch of the projector, Fig. 3, is taken from there.

III. METHOD OF ANALYSIS OF EVENTS

Because of the large solid angle of observation, the cloud chamber offers possibilities for obtaining more information concerning stars from a pure substance than does any other single experimental device. It enables one to study individual events in detail, and with the aid of a stereoscopic camera and projector it permits

reproduction of each track in its original size, shape and position. With the addition of a magnetic field one can gain information about the momentum and energy of each particle.

1. Available Data

Following an outline by J. Tracy[9], the data available for analyzing an event in this investigation may be divided into three categories. These are:

General Experimental Data. This includes knowledge of the direction and approximate energy distribution of the neutron beam, the direction and strength of the cloud chamber magnetic field, and the composition and stopping power of the gas mixture in the cloud chamber.

Individual Star Data. This includes information obtained from measurements on the individual events, such as initial radius of curvature, density, initial direction, range, rate of change of curvature and rate of change of density.

Auxiliary Information. This includes application of the laws of conservation of momentum, energy, mass and charge, as well as knowledge of range-energy relations, specific ionization vs. energy relations and characteristic track endings.

2. Identification Procedure

On the average, three two-prong stars and about an equal number of heavily-ionizing single tracks appear in each picture. The possible reactions when a neutron strikes a helium nucleus are as follows:

INELASTIC $${}_0n^1 + {}_2He^4 \longrightarrow {}_1H^2 + {}_1H^3 \qquad (dt)$$

$$\longrightarrow {}_1H^2 + {}_1H^2 + {}_0n^1 \qquad (dd)$$

$$\longrightarrow {}_1H^1 + {}_1H^3 + {}_0n^1 \qquad (pt)$$

$$\longrightarrow {}_1H^1 + {}_1H^2 + 2{}_0n^1 \qquad (pd)$$

$$\longrightarrow {}_1H^1 + {}_1H^1 + 3{}_0n^1 \qquad (pp)$$

$$\longrightarrow {}_2He^3 + 2{}_0n^1 \qquad (He^3)$$

ELASTIC $$\longrightarrow {}_2He^4 + {}_0n^1 \qquad (He^4)$$

Stars with three or more prongs are observed occasionally; they are due to oxygen nuclei in the water vapor. From the partial pressures existing in the chamber immediately after expansion, the relative number of oxygen nuclei can be computed, and in a later section this will be compared with the relative number of helium and oxygen stars observed. Analysis of an event involving the helium nucleus requires identification of protons, deuterons, tritons, He^3's and He^4's.

Two-Prong Stars. The identification of the particles involved in the two-prong stars rests mainly on measurement of their radii of curvature and an estimate of their relative ionizations. If one knows the strength of the magnetic field at the position of the track, two out of the following three quantities determine the third: Particle identity, curvature, ionization. A two-prong star from helium can include only singly charged particles, and over the range of energies observed in this experiment a simple rule holds. For a given radius of curvature the ionization of a deuteron is approximately three times that produced by a proton and of a triton is six times that for a proton. A table was constructed which gives $H\rho$ vs. ionization for p, d, t, He^3, and He^4; it is reproduced in full in APPENDIX IV. The table is used in the identification of a track in the following manner: the ionization of the particle is bracketed between two proton tracks in the background; that is, if the

track is lighter than one of the proton tracks and heavier than the other, and the proton densities are sufficiently close together, the particle identity is uniquely determined in its proper $H\rho$ row in the table.

A start can be made in finding a reference ionization density if one recognizes that in each picture a more or less parallel beam of lightly ionizing particles comes through the entrance window with radii around 35 cm. The fact that the ionization of these tracks is the lightest observed for these curvatures plus the fact that occasionally tracks are observed to come in with these curvatures which appear denser but never lighter, establishes these background tracks as protons. This verifies the expectation that protons are knocked out of the walls of the collimator and window by the incident neutrons. Since their identities and curvatures are established, their ionizations can be obtained from the table.

Various other aids can be employed in identifying particles. If, for example, one prong of a star is a deuteron and the two prongs are not coplanar with the incident neutron beam direction, then the other prong cannot be a triton. Or, one prong may end in the chamber giving a rise to a characteristic ending. The ending of a track in a magnetic field is characteristic because a unique theoretical relation exists for each particle which relates $H\rho$ vs. residual range. The ending of the track in question can be compared with the theoretically computed track shape or with an experimental characteristic ending in the same gas mixture which has previously been well established from other evidence. Characteristic endings are shown in APPENDIX II.

By such reference and bracketing procedures it has been possible to identify the fragments from two-prong stars in most cases. Out of 179 two-prong stars whose tracks lay within angles of $\pm 30^{\circ}$ to the horizontal plane, eight could not be analyzed with certainty. Of these eight, four had one or both prongs too short, and four were either pd's or pt's. The latter uncertainty stems from the fact that when a track has an ionization with respect to minimum starting at about 75, it is very difficult to decide whether the ionization is 75 or twice as much. In about 10 percent of the cases the two-prong stars had a track whose identification presented some difficulty due to one or more of the following: the tracks were near the edge of the chamber or illuminated region and were thus too short, or they had a fuzzy appearance due to improper timing, or a track was partially obscured by clouds of water vapor. In these doubtful cases a statement was made of the more likely interpretation; a second observer was asked to make the same type of decision independently. In all doubtful cases there was agreement.

It must be mentioned that the term relative ionization has been used loosely for apparent track density. Actually it is apparent track density that is observed, and many variable factors enter into the relation between ionization and apparent track density -- such as chamber illumination, expansion ratio (moisture available for drop formation), dip angle α, time of passage of particle through the chamber after expansion, and width of track. Obviously the greatest chance of success can be expected in the identification procedure when those tracks are compared which have these factors most nearly alike. In general, the ionization of light tracks could be estimated

to within a factor of 1.5, medium tracks to about 2, and heavy tracks (which differed in width rather than blackness) to 3-4.

One-Prong Stars. The single tracks from helium are He^3's and He^4 recoils. These tracks turn out to be most frequently of low energy and they will then inevitably be extremely heavy and often also short. Ionization estimates fall in the range above 100 where estimates of density are insufficiently accurate. Thus He^3 and He^4 cannot be differentiated by their densities because when a He^3 and He^4 have the same curvature, the table in APPENDIX IV shows that the ionization of He^4 is about 3/2 times that of He^3. However, if the track ends in the chamber, its change of radius with residual range can be ascertained and the track can be compared with a characteristic ending. If the track does not end in the chamber, the change in radius along the track is insufficient to determine whether it is He^3 or He^4. Also because of the large energy spread of the neutrons there exists no condition which can be deduced from the kinematics that would distinguish the particles with certain energies and angles. The assumptions that have to be made because of this lack of experimental information will be discussed in a subsequent section.

Stopping Power. A check was made of the range-energy relations expected from the calculated stopping power of the gas mixture in the chamber. Immediately after expansion, the chamber contained 79.7 cm helium and 1.4 cm water vapor. From this the stopping power of the mixture was computed to be 0.185 relative to dry air at 760 mm and 15° C. The energies of a few long proton tracks ending in the chamber were determined from $H\rho$ measurements and their ranges measured with

a long flexible ruler. The calculated and measured ranges agreed to within 5-10 percent, which is well within the experimental error expected.

APPENDIX II gives a sample analysis of two pictures and shows characteristic track endings.

3. Errors in Measurement

Analysis of an event involves, besides identification of the particles, measurements of radius of curvature, dip angle, beam angle, height of track in the chamber, distance of track from center of chamber, range (when track ends), and magnetic field strength. (For definitions, see APPENDIX I).

Radius of Curvature. The curvature of a track is measured by reprojecting it life-size on a translucent screen, which is rotated in space until it contains the plane of the track (called the slant plane in Fig. 3), and then matching it with one of a series of arcs ruled on a Lucite template. In a number of past experiments experience has shown that the error made in curvature measurements always amounts to 0.1 mm error in the sagitta irrespective of the particular curvature and track length available. One can conclude from inspection of tracks which were made with no magnetic field that errors in curvature due to turbulence were negligible in comparison to measurement uncertainties.

Dip Angle and Beam Angle. The whole question of accuracy of reprojection and measurement with the apparatus employed in this experiment has been thoroughly investigated by W. Powell and collaborators[8]. They concluded that dip angles could be determined to within $\pm$ 1 1/2° for $0 < \delta < 50^\circ$, and beam angles to $\pm$ 1°. The latter uncertainty includes the systematic error in aligning the line drawn

on the top glass of the chamber (which appears in every picture) with the direction of the neutron beam, as well as the error in measurement. All dip angle and beam angle measurements rest on the assumption that the incident neutrons entered the chamber in a parallel beam. This assumption is verified by the fact that the number of stars produced outside the volume swept out by the neutron beam is negligible.

Complete analysis of stars was limited to those events which had all their prongs lying within dip angles less than $\pm 30^{\circ}$. This restriction was necessary because when the prong under consideration is too slanted, accurate measurement of curvature and dip angle is impossible in a large number of cases. Under those conditions the track is usually short because it quickly passes out of the lighted region, and the extreme stereoscopic effect required of the lenses makes the superposition of the two images insensitive to variations of the slant plane. Imposition of this restriction necessitated an extended correction procedure, which is discussed in detail in the section on CORRECTIONS.

Magnetic Field. The nominal value of the magnetic field strength in each picture was obtained from an ammeter which is photographed simultaneously and from a magnetization curve. The magnetic field varies by 6 percent over the region where tracks were measured. The strength of the field at the center of the measured part of the track was determined from an accurate map of the field which varies sufficiently slowly so that second order corrections for changes of the magnetic field along the track were negligible.

4. Calculations

Once a particular event has been measured, the analysis is completed by making the appropriate calculations. The following table shows an example of the quantities computed for each star:

TABLE I

Prong	Particle	$H_\rho \times 10^5$	Mev	θ	ϕ	$H_{\rho t}$	$H_{\rho z}$	$E_{n'}$	E_n
A	d	17.47	70.8	4°	225°	-1.22	17.44	92.7 Mev	90.0 Mev
B	t	3.26	1.7	162°	37°	1.03	-3.09		
C	p	8.14	31.3	36°	227°	-4.85	6.54	4.1 Mev	75.7 Mev
D	d	7.73	14.4	69°	32°	7.24	2.72		
E	p	3.54	6.0	93°	336°	3.54	-0.17	25.1 Mev	61.9 Mev
F	t	8.23	11.0	19°	19°	2.68	7.79		
G	p	5.88	16.3	44°	12°	4.12	4.19	41.2 Mev	83.6 Mev
H	t	6.24	6.2	42°	313°	4.13	4.08		
I	He^4	Range 5.7 cm	2.1	75°	209°				49.1 Mev
II	He^4	" 4.4 cm	1.2	42°	146°				3.4 Mev

$H_\rho \times 10^5$ is the momentum of the particle in gauss - cm if it has only one charge and is of course independent of the singly-charged particle's identity. The energy of the particle in Mev is computed from $H_\rho \times 10^5$ by means of the proper conversion formula.* The scatter angle θ and azimuthal angle ϕ are computed from the measured dip angle α and beam angle β. (See APPENDIX I.) $H_{\rho t}$ and $H_{\rho z}$ are the components of the momentum of the particle transverse to the beam and along the beam direction.

Two-Prong Stars. Since the disintegration of helium by a neutron into a deuteron and a triton is a two-body problem, the energy of the incident neutron can be calculated in two ways -- momentum balance and energy conservation. These computed energies are entered in the columns $E_{n'}$ and E_n respectively, and should be equal. The two-body feature of this case can be checked in two other ways. The transverse momenta of the triton and deuteron must be equal and opposite; and the azimuthal angles of the deuteron and triton must be 180° apart. These requirements are generally satisfied to within

---

* Tables and graphs kindly supplied by J. de Pangher.

5 percent, except in occasional situations when one of the tracks is short and therefore difficult to measure, or one of the computed quantities depends very sensitively on a measured angle.

In the case of pt and dd disintegrations, in which one secondary neutron comes off, it is still possible to calculate the energy of the incident neutron. The unknown quantities are the two momentum components of the ejected neutron and the energy of the incident neutron (since its direction is known). The three available relations are energy and momentum conservation. $E_{n'}$ stands here for the energy of the ejected neutron and E_n for the energy of the incident neutron.

In the case of pd disintegrations two neutrons come off in addition to the proton and deuteron, and there are too many unknowns for the solution of the problem. A minimum value for the energy of the incident neutron can be extracted, however, if the two ejected neutrons are lumped together and treated as a particle with two neutron mass units with the requisite momentum to balance the problem. This arises from the fact that the energy associated with the momentum of this lumped particle is less than the energy associated with the separate neutron momenta. Consequently, in the table $E_{n'}$ represents the energy of the lumped particle and E_n the minimum energy of the incident neutron.

No calculations can be made for pp events since three additional neutrons come off. Only three pp cases have been observed in the whole investigation.

APPENDIX III contains the derivations of the formulas used in the above calculations.

<u>He^4 Recoils</u>. The measured energy of a He^4 recoil in elastic scattering leads directly to the energy of the incident neutron;

namely

$$E_n = \frac{25}{16} \frac{E}{\cos^2 \theta},$$

where E is the energy of the He^4 recoiling at an angle θ. The corresponding scatter angle γ of the neutron is given by

$$\cot \gamma = \frac{5}{8 \cos \theta \sin \theta} - \frac{1}{\tan \theta} .$$

It is independent of the particular He^4 recoil energy because the speed of the recoiling He^4 in the c.m. system is equal to the speed of the c.m. system with respect to the laboratory frame.

IV. CORRECTIONS

A number of corrections must be applied to the data as taken off the film. These involve geometrical factors due to the inherent blindness in some regions in stereoscopic viewing, as well as assumptions concerning the theory in order to circumvent certain experimental limitations in the identification procedure.

1. Single-Prong Stars

In the first place, only those events have been measured whose tracks lay within an angle of $\pm 30°$ to the horizontal plane containing the neutron beam. In order to find the number of events which would have been observed without this restriction on α, a weighting factor has to be assigned to each event. This factor is the reciprocal of the fraction of total solid angle available to the track if one uses the assumption of isotropic azimuthal distribution about the direction of the neutron beam. One must compute what fraction of the azimuthal angle ϕ* meets the requirement at a given scatter

---

* All angles are defined in APPENDIX I.

angle θ that the dip angle α be limited to $\pm 30^\circ$. In Fig. 4 the direction in space of any track is given by a point in the $\phi - \theta$ plane; the oval regions are defined by the equation

$$\sin \phi = \frac{\sin \alpha}{\sin \theta} ,$$

with $\sin \alpha = \pm 1/2$. The interpretation of the plot is this: a track with a given scatter angle θ would be measured (i.e. would have $\alpha < \pm 30^\circ$) for those azimuthal angles ϕ which fall outside the oval regions. Consequently the probability of observing a track when it has a given scatter angle θ is simply the ratio of the number of ϕ degrees outside the ovals to 360 degrees. The weighting factor is the reciprocal of this fraction, and its maximum value, which occurs at $\theta = 90^\circ$, is 3.0 The appropriate correction factor was applied to each track individually.

2. Two-Prong Stars

In the case of events with two prongs the correction procedure is complicated by the fact that the rejection of an event may be due to one or both prongs lying outside the $\pm 30^\circ$ limit; and, furthermore, the fraction of total solid angle available to the event depends on the difference in azimuthal angles of the two tracks ($\Delta \phi$). From the plot in Fig. 4 a table was constructed graphically which lists the solid angle correction factor for a given θ_1 (prong 1), θ_2 (prong 2) and $\Delta \phi$. (These three parameters geometrically define a two-prong event on the assumption of azimuthal symmetry.) The procedure used was this: one leg of a pair of dividers was always kept on θ_1 while the other leg was always kept on θ_2. The angle between the legs fixed the parameter $\Delta \phi$. The dividers then were moved vertically up the plot so that θ_1 moved from $\phi = 0^\circ$ to $\phi = 360^\circ$.

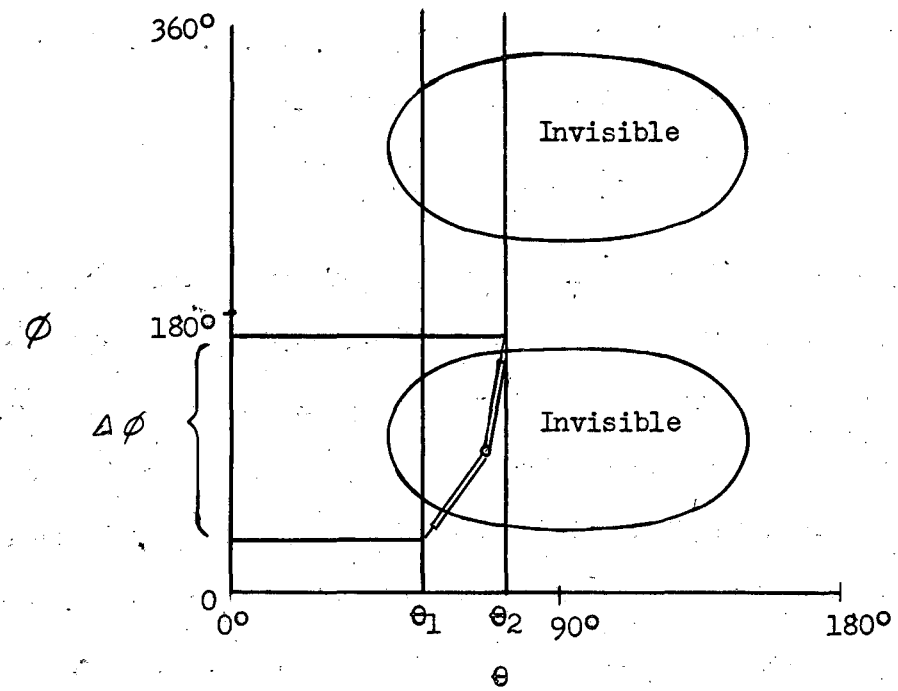

Every time one or the other leg crossed into or out of the invisible regions the fact was recorded. Thus it was found what the probabilities are that one or both prongs are not measurable for a given θ_1, θ_2 and $\Delta\phi$. From this information one could then calculate two correction factors. One correction factor gives the number of events to be expected in the azimuthal region where one prong is too slanted; the other gives the number where both prongs are too slanted. The sum of the measured event and the two correction factors is the number of events which would have been observed if there had been no restriction on δ.

As a check on this computed correction procedure, the events for which one or both prongs lay outside the ± 30° limit have been counted, and whenever possible, identified. The total number of these partially analyzed stars plus the total number of

completely analyzed stars should be equal, within statistical errors, to the number of completely analyzed stars corrected by the computed solid angle correction. Such a check would assure one that nothing significant was overlooked by confining α to $\pm 30^{\circ}$. For certain few two-prong stars both prongs would never fall inside the 30° limits regardless of how the configuration was rotated about the beam axis. This situation would amount to an infinite computed solid angle correction factor, but it will be shown that no significant contributions could have come from these types of stars. In practice the correction factors turned out to be below 3.0 and a few went as high as 6.0.

3. The He^3 Assumption

As has been pointed out before, it was impossible to determine whether a single track was He^3 or He^4 when it did not end in the chamber. In order to estimate what fraction of all the single tracks were He^3's, some assumption must be made regarding the He^3 formation process.

The pt and He^3 events can be considered as similar processes -- in one case the incoming neutron interacts with and strips a proton off the helium nucleus, while in the second case it strips off a neutron. As an approximation then, it seems reasonable to expect the ratio of He^3 to pt events to be the same as the ratio of the n-n cross section to the n-p cross section at 90 Mev. To the extent of present knowledge, the numerical value of σ_{pp} must be employed for σ_{nn}. Then the ratio of σ_{nn} to σ_{np} becomes about 1/3[10].

Furthermore, those cases of the dt events in which a pick-up deuteron comes off in the forward direction must be included as a

type of pt event becuase the deuteron is actually not formed until some time after the disintegration[4]. Since in about one-half of all the dt events a high-energy deuteron comes off in the forward direction, the procedure proposed for estimating the number of He^3 events is

$$1/3 \text{ (no. of pt events} + 1/2 \text{ no. of dt events).}$$

V. RESULTS AND DISCUSSION

1. Inelastic Events

TABLE II

		pt	dt	pd	dd	pp	He^3	Total
1	Measured	88	33	31	17	2		171
2	Not Identified	5.1	0.8	1.7	0.4			8
3	Sum	93.1	33.8	32.7	17.4	2		179
4	Corrected Total	212.6	75.5	76.3	37.0	3.8		
5	Total with He^3 Assumption	212.6	75.5	76.3	37.0	3.8	83.5	488.7
6	Total for Neutrons >40 Mev	209.1	66.5	76.3	35.2	3.8	80.8	471.7
7	Probable Error	7.3%	12.3%	12.1%	16.8%	48%		5.2%

The first row in TABLE II shows the inelastic events which had dip angles less than $\pm 30^\circ$ and were thus subject to a detailed analysis. In addition there were four stars (previously discussed) which could not be identified and four stars where the interpretation could have been either pd's or pt's (also previously discussed). These eight unidentified events were arbitrarily divided into groups with the same relative distribution as the identified events in the first row. The numbers in the second row show the grouping of these eight events.

Line 3 is the sum of line 1 and line 2. The fourth row gives the total number of events of each type which would have been observed

if α had not been restricted to less than $\pm 30^{\circ}$. This correction is discussed in detail in the next two sections.

The fifth row shows the total number of inelastic events of each type including 83.5 events for He^3 obtained by using the assumption made in the section on CORRECTIONS.

Row 6 is the same as row 5 except it includes only events from neutrons above 40 Mev.

Line 7 gives the statistical probable error based on events actually analyzed from neutrons above 40 Mev.

Results of Solid Angle Corrections. If it were true that all types of stars appeared in the 30° group, then a solid angle correction factor could be applied to each analyzed star in the 30° group which would give the number of stars which would have been observed if α had not been limited. However, if there is a class of stars which would never have both prongs within the 30° limit (irrespective of the rotation of the configuration about the beam axis), some other method must be used to reveal this class of stars.

Now, stars with one or both prongs with dip angles greater than 30° could be recognized and counted, but not completely analyzed. TABLE III shows the results of this partial analysis.

TABLE III

	pt	it	pd	dd	pp	p?	d?	t?	??	Total
One prong $\alpha > 30^{\circ}$	51	17	14	12	1	35	25	14	7	176
Both prongs $\alpha > 30^{\circ}$	10	3	2	1	0	1	3	5	16	41
Total	61	20	16	13	1	36	28	19	23	217

The question marks (?) denote unidentified prongs. For purposes of comparison, the events containing one or both unidentified prongs are arbitrarily divided into groups with the same relative distribution as the identified events in TABLE III and added to the identified events. The results of this distribution appear in TABLE IV.

TABLE IV

	pt	dt	pd	dd	pp	Total
One prong $\alpha > 30^\circ$	92.8	29.5	28.9	23.8	1	176.0
Both prongs $\alpha > 30^\circ$	24.6	8.5	5.1	2.9	0	41.1
Total	117.4	38.0	34.0	26.7	1	217.1

As was described previously, the computed solid angle correction factor could be broken up into two parts -- one factor correcting the 30° group analyzed events for those solid angles in which one prong lay outside, and another factor correcting the analyzed events for those solid angles in which both prongs lay outside. In TABLE V the net corrections obtained by applying a computed solid angle factor individually to each analyzed event in the first row of TABLE I are compared with the partially analyzed events from TABLE IV.

TABLE V

		pt	dt	pd	dd	pp	Total
One prong $\alpha > 30^\circ$	Partially Analyzed	92.8	29.5	28.9	23.8	1	176.0
	Computed	97.3	35.8	37.7	16.3	1.8	188.9
Both prongs $\alpha > 30^\circ$	Partially Analyzed	24.6	8.5	5.1	2.9	0	41.1
	Computed	22.2	5.9	5.9	3.3	0	37.3
Total	Partially Analyzed	117.4	38.0	34.0	26.7	1	217.1
	Computed	119.5	41.7	43.6	19.6	1.8	226.2

Discussion of Solid Angle Corrections. It is proper at this point to present evidence that no significant information was missed due to the fact that some stars could have had "unusual" configurations so as to have both prongs always outside the 30° limits.

(1) TABLE V shows that the correction of 226.2 events as computed from application of solid angle corrections to the analyzed stars in the 30° group is equal, within statistical error, to the 217.1 counted events outside the 30° limits. This proves that the number of "unusual" stars must be small.

(2) The stars analyzed in the 30° group yield a certain distribution of events. The 111 stars that were successfully analyzed in the group having one or both prongs outside (TABLE III) have the same distribution of events -- as follows:

	pt	dt	pd	dd	pp
Analyzed $\alpha < \pm 30^{\circ}$	52%	19%	18%	10%	1%
Analyzed $\alpha > \pm 30^{\circ}$	55%	18%	14.5%	11.5%	1%

(3) The 106 stars left in TABLE III with one or both prongs unidentified can be arranged so as to give the same distribution.

Hence one can conclude that it is highly unlikely that there is any considerable number of stars of an "unusual" character among the 106 stars of item (3) whose presence would change the distribution in item (2) by a significant amount.

In TABLE I line 4 gives the number of corrected events. This number was obtained by adding to the events in line 3 the total computed solid angle corrections from TABLE V. This procedure is justified

in view of the above arguments.

2. Elastic Events

The following table shows the results of measurements of the single prong stars.

TABLE VI

He^4's ending in the chamber	139
Single tracks not ending	125
He^3's ending	2
Tracks less than 2 cm long	105
Tracks counted, with $\alpha > \pm 30^\circ$ (ending and not ending)	349
Compute solid angle correction to He^4's ending	218
Compute solid angle correction to tracks not ending	127
Weighted single prong events due to neutrons > 40 Mev	441

One has to determine now the number of single tracks which would have been observed if all solid angles had been looked at and if no tracks had been missed because they were too short. In order to correct for the solid angle limitation, a proper weighting factor has been applied to each individual event -- as explained in detail previously. The angular distribution of the scattered neutrons, see Fig. 7, shows a lack of neutrons in the forward direction, which is due to the short range of the recoils. It is proposed to extrapolate the experimental spectrum to zero scatter angle according to a reasonable theoretical assumption as to the shape of the spectrum, and it will be shown that 124 He^4 events from neutrons above 40 Mev are contributed by this extrapolation.

If the total number of neutron-helium collisions is to be normalized to the total n-He^4 cross section as determined indirectly by carbon disk detectors, those helium collisions must be excluded which were due to neutrons not present in the total cross section experiment beam. The carbon activation reaction has a threshold at 20 Mev, and the number of neutrons detected between 20 and 40 Mev is small because of the sharp drop of the activation curve near the threshold and the small number of neutrons in that part of the spectrum(11). Hence no serious error is introduced if only helium events from neutrons above 40 Mev are included in the normalization. There are very few inelastic events from neutrons between 20 and 40 Mev (see TABLE II) -- the thresholds range from 17.5 Mev to 25.9 Mev -- and it will be shown that it is not feasible to correct for missed short tracks from neutrons below 40 Mev.

In order to obtain the estimated number of He^4 events, the 124 extrapolated He^4 events are added to the 441 events appearing in TABLE VI. Finally the 80.8 He^3's, which have been assumed to occur with the inelastic events (TABLE II) must be subtracted out. Thus the total number of He^4's is

$$441 + 124 - 80.8 = 484.$$

It should be noted that the normalization of the total number of helium collisions (inelastic and elastic) is independent of the He^3 assumption. The assumed 80.8 He^3 events which have been added to the inelastic events are subtracted out from the single prong events, leaving the total number of events unchanged.

In order to examine the question of why only two He^3's were observed ending in the chamber, one can again consider the analogy

between the He^3 and pt processes. The following ratios are then of interest:

Number of He^3's ending to number of He^3's not ending as based on the He^3 assumption 2/39

Number of tritons ending to number of tritons not ending in the pt processes 20/88

Any one of the following reasons could account for the small number of He^3's observed to end:

(1) The number of He^3's was grossly overestimated in the He^3 assumption.

(2) It is a special feature of the $n(He^4, He^3)2n$ reaction that no low energy He^3's are emitted. (They would have to have less than a few Mev in order to end in the chamber.)

(3) More than two He^3's did end in the chamber but they were confused with He^4's. (This would only be a possibility if the He^3 tracks were consistently short.)

As far as possibility (3) is concerned, it should be noted that for a given energy the range of a He^3 is only about one third that of a triton. The ranges of 17 out of the 20 tritons which ended were such that if the particle had been a He^3 with the same energy, its range would have been less than 3 cm, and in such case it could have been confused with He^4. Whether or not some He^3's should have had the proper energy to end in the chamber depends of course on the energy distribution of the He^3's, and one can only speculate what this might be from comparison with the triton energy distribution from pt events (shown in Fig. 11).

3. <u>Cross Sections</u>

In order to obtain absolute cross sections the total number

of events (472 inelastic + 484 elastic), for incident neutrons above 40 Mev, is normalized to the interpolated n-He^4 total cross section from the work of Cook et al.[11]. When σ is plotted vs. $A^{2/3}$ for H, D, Li and Be, σ for He turns out to be 1.9×10^{-25} cm^2 when the points are connected by a smooth curve. A probable error of 10 percent is arbitrarily assigned to this value.

On the basis of the INELASTIC and ELASTIC events listed, the results are

$$\sigma_{elastic} = 96 \pm 17 \text{ mb}$$

$$\sigma_{pt} = 42 \pm 6 \text{ mb}$$

$$\sigma_{dt} = 13 \pm 2.5 \text{ mb}$$

$$\sigma_{pd} = 15 \pm 2.5 \text{ mb}$$

$$\sigma_{dd} = 7 \pm 1.5 \text{ mb}$$

$$\sigma_{pp} = 0.8 \pm 0.4 \text{ mb}$$

$$\sigma_{He^3} = 16 \text{ mb (assumed)}$$

The ratio of $\frac{\sigma_{inelastic}}{\sigma_{total}}$ is 0.49 ± 0.07

4. Errors

The errors quoted in TABLE II are the statistical probable errors based on the number of events actually analyzed. For each quantity making up the 484 elastic events a statistical probable error can be associated based on the number of events actually measured. But it is more realistic to consider the magnitude of the extrapolation that had to be made for missed tracks and the uncertainty in the 80.8 assumed He^3 events, and consequently a probable error of $\pm$ 60 was assigned to the 484 recoils.

The uncertainties arising from the identification procedure have been discussed in the section METHOD OF ANALYSIS OF EVENTS.

5. Comparison With Theory

In 1950 Heidmann published an analysis of the 90 Mev neutron-helium scattering problem[12]; it is interesting to compare his predictions for the relative cross sections with the present experimental findings.

Process	Theory[12]	Theory Revised[13]	Experiment
Elastic He^4	180 mb	160 mb	96 ± 17 mb
pt	63	60 ± 10	42 ± 6
dt	16	16	13 ± 2.5
pd	~0	~2	15 ± 2.5
dd	~0	~0	7 ± 1.5
pp	~0	~0	0.8 ± 0.4
He^3	6	~6	16 (assumed)

If Heidmann's revised theoretical results were diminished by the ratio $\frac{190 \text{ mb}}{244 \text{ mb}}$ so as to make his total cross section equal to the interpolated experimental value, the agreement would be excellent for the He^4, pt and dt modes of disintegration. In any case the agreement is remarkable because, as the author himself points out, the calculations should be criticized for use of gaussian functions for the potential and for the use of deuteron wave functions, which were employed to simplify the integrations. Heidmann apparently underestimates the occurrence of the pd and dd processes, but agrees that complete disintegration of helium by a neutron (pp) is rare.

In arriving at the number of He^3 disintegrations, Heidmann was the first to consider the pt and He^3 events as similar processes. However, he estimated that the number of He^3 to pt events would be given by

$$\frac{1/4}{1/4 + 3/4} \left(\frac{V_{singlet}}{V_{triplet}}\right)^2,$$

or about one tenth. As discussed in the section on CORRECTIONS, in the present investigation the ratio of He^3 to pt events is assumed to be

$$\frac{\sigma_{np}}{\sigma_{nn}} = \frac{\sigma_{np}}{\sigma_{pp}} = \frac{1}{3},$$

which leads to about three times the He^3 cross section. Only the He^3 and He^4 cross sections and the ratio $\sigma_{inelastic}/\sigma_{total}$ are affected if one uses one or the other assumption. One piece of evidence which speaks in favor of the 1/3 ratio comes from n-d scattering at 90 Mev. W. Powell[7] found that the cross section for the production of protons with less than 10 Mev is 14.6 mb and that for protons with more than 10 Mev is 51.1 mb. The low energy protons are roughly isotropic and are left behind when the incident neutron hits the neutron in the deuteron, while the higher energy protons come off predominantly forward and result from the incident neutron striking the proton in the deuteron. The ratio between these two processes, which can be considered as n-n and n-p interactions in a light nucleus, is 1/3.

6. Energy Dependence

The incident neutron spectrum as measured from He^4 recoils ending in the chamber is shown by the single points in Fig. 5. If all the single tracks which do not end in the chamber are included, the upper curve results. It is seen to have a quite similar shape, which is to be expected since the He^3's have been estimated to constitute only about 10 percent of the spectrum. (Of course below 20.5 Mev the events must all be due to He^4 since this is the threshold for

the $He^4(n, 2n)He^3$ reaction.) The peak occurs at about 70 ± 5 Mev. The distribution has the general features resulting experimentally from the deuteron stripping process, namely a peak near half the deuteron energy and a peak of low energy neutrons. The low energy peak is undoubtedly exaggerated due to the rapid increase of the elastic scattering cross section with decreasing neutron energy. The broadness of the spectrum and the shift of the peak down to 70 Mev is due to the fact that the stripping target used in this part of the experiment was 2 in. Be rather than the more desirable 1/2 in. Be. It can be concluded from the distribution that the energy dependence of the elastic scattering is not very pronounced in the region from 40 to 100 Mev.

For the various inelastic processes, the number of events vs. incident neutron energy is plotted in Fig. 6; the peaks occur at about

pt	75 ± 5 Mev
dt	65 ± 5 Mev
pd	67 ± 5 Mev

(The neutron energy in the pd cases is a minimum).

Since the incident neutron spectrum was the same in each case, the qualitative nature of the curves can be compared. The small shift of the pd curve to lower energies with respect to the pt curve may simply reflect the fact that the calculated value of the neutron energy gives a minimum value only. The dt curve shows a decided energy dependence, and this agrees with the sharp falling off with energy of the pick-up process which is theoretically expected. Preliminary experimental results on n-d pick-up deuterons verify this sharp energy dependence[14].

7. Energy and Angular Distributions

Elastically Scattered Neutrons. The elastic events were divided into two groups -- those due to incident neutrons below 40 Mev and those due to incident neutrons above 40 Mev. The reasons for this division are first that there exists evidence that low energy neutrons scatter from helium in a different manner than high energy neutrons(15); second to be able to make a comparison with theory, in particular that due to Heidmann(12); and third for a reason which will become evident in the next paragraphs.

The points denoted by triangles in Fig. 7 show the angular distribution of elastically scattered neutrons ($d\sigma/d\theta$) from incident neutrons with energies greater than 40 Mev; the points denoted by circles were obtained by dividing the $d\sigma/d\theta$ points by the average value of the sine over the 15° intervals and represent thus $d\sigma/d\Omega$. By having proceeded on the basis that all single prongs not ending in the chamber are He^4's, little error was made since only about 16 percent of the events above 40 Mev is contributed by He^3's. Evidently there is a hole in the experimental distribution near the forward direction; it is due to the corresponding recoils being too short to be measured with certainty.

According to Heidmann's theory the angular distribution of 90 Mev elastically scattered neutrons is a gaussian curve centered on the forward direction. His predicted curve has the equation

$$\frac{d\sigma}{d\Omega} = 4.50\ e^{-7.86\theta^2} \times 10^{-25} cm^2$$

in the c.m. system. Since the present experimental data are not incompatible with a gaussian, it was decided to draw a gaussian curve through the experimental points; its form is

$$\frac{d\sigma}{d\Omega} = Ke^{-5.0\theta^2}$$

It is shown by the solid line in Fig. 7 and was extrapolated to zero degrees scatter angle.

Advantage has been taken previously of the opportunity to associate the events under the extrapolated part of the curve with the events missed because the tracks were too short. The area under the extrapolated part of the curve contributes 168 events lumped into the 0-15° scatter angle group ($d\sigma/d\Omega \sin\theta$). The reason why the angular distribution was plotted in 15° groups in the first place is that when a 40 Mev neutron is scattered at 15°, the corresponding recoil will just be 2 cm long. (This was the criterion selected below which recoils were merely counted instead of measured.) Consequently one begins to lose measurable tracks for neutron scatter angles of 15° and less. The critical alpha recoil angle corresponding to the neutron scatter angle of 15° is 80.5°. Recoils have been observed at angles as high as 84°; they are due to neutrons of energies higher than 40 Mev.

From the 168 extrapolated events in the 0-15° group, 44 weighted events must be subtracted since they were actually observed and measured. The remaining 124 events were then added to the observed single prong tracks.

Fig. 8 shows the angular distribution of elastically scattered neutrons from incident neutrons with energies less than 40 Mev. Here again a substantial number of neutrons are known to be missing near the forward direction. But since they can be missing up to fairly large neutron scatter angles (when a 5 Mev neutron is scattered at 45°, its alpha recoil will just be 2 cm long), it is not

possible to estimate the distribution of the missing tracks. However, the distribution confirms the general trend found by Swartz[15] that elastic scattering is peaked less in the forward direction at lower energies. The picture is qualitatively that the forward peak of diffraction scattering on the basis of the opaque nucleus model is spread out at lower energies, and that more nearly isotropic scattering is approached.

The $He^4(n, d)t$ Reaction. The angular distribution of deuterons from dt events is plotted in Fig. 9 and shows the expected peak of pick-up deuterons in the forward direction. The distribution is plotted both in terms of $d\sigma/d\theta$ and $d\sigma/d\Omega$. The solid line representing the differential cross section $d\sigma/d\Omega$ is subject to some error due to the inaccuracy introduced by averaging sin θ over a 30° interval; but it is included to show the approximate half-width of the forward cross section, which is estimated to be 25°. On the other hand, the $d\sigma/d\theta$ points are useful in comparing the relative forward to backward scattering; they show that the events under the peak constitute about one-half of the total dt cross section. Heidmann has pointed out[13] that the critical tests between theory and experiment are, in order of increasing sensitivity to large momentum changes (and thus small interaction distances): the total dt cross section, the angular half-width of fast forward deuterons, and the ratio of forward to backward deuterons. The following is a comparison between theory and experiment on these points:

	Theory	Experiment
Total σ_{dt}	16 mb	13 ± 2.2 mb
Half-width	8.4°	~25°

	Theory	Experiment
Ratio $\frac{\text{forward}}{\text{backward}}$ *	1000/1	1/1

The discrepancies increase exactly in the order listed above, with only the total σ_{dt} being in satisfactory agreement. One possible source of the discrepancies has already been mentioned, namely the use of the gaussian function for the potential in the calculations.

The one event plotted in the 165° group is a low energy deuteron with an associated triton going forward with 75 Mev. The process responsible for this is undoubtedly triton pick-up.

In Fig. 10 the energy distribution of the deuterons from dt events is plotted. The peak corresponding to pick-up deuterons falls at 50 Mev. Although the dt process is a two-body problem, there is no one to one correspondence between a point on the angular distribution plot and a point on the energy distribution plot because of the variety of energies of the incident neutrons. This fact, incidentally, must be kept in mind in making all comparisons with Heidmann's theory, since he analyzed the problem for monochromatic 90 Mev incident neutrons.

<u>The $He^4(n, pn)t$ Reaction</u>. According to Heidmann's prediction the tritons from the pt reaction are of low energy (2 Mev on the average) and are distributed almost isotropically. Fig. 11 shows the energy distribution of the tritons, and agreement is seen to be excellent. However, Fig. 12 shows that the angular distribution of the tritons is not isotropic but concentrated in the forward direction. The proton energy distribution is shown in Fig. 13.

---

* Strictly, the experimental ratio observed is pick-up deuterons to non-pick-up deuterons.

The proton angular distribution from pt events is plotted in Fig. 14 together with the proton angular distribution from pd events. In both distributions it can be said that the free nucleon n-p scattering is reflected to some extent. This would be expected on the basis of a model first proposed by Goldberger[3] the general features of which were verified by Hadley and York[2]. According to this picture, the bombarding particle interacts with an individual nucleon rather than with the struck nucleus as a whole, and probably leading to the ejection of a fast particle in the forward direction.

Fig. 15 gives the energy distribution of protons from pd events. The statistics are not good because of the low frequency of occurrence of this type of event. Nor does any theory exist at present with which comparison can be made.

8. Oxygen Stars

Since a small number of oxygen stars is an unavoidable by-product of this experiment, it is desirable to make a comparison between the number of oxygen events expected and observed. The following table shows the distribution of oxygen stars observed and also that found by Tracy and Powell[5].

Prongs	Experiment	Tracy and Powell
1	6	
2	14	14 + ?
3	14	20
4	8	8
5	2	6
?	2	

As mentioned in the first section, the ratio of helium to oxygen nuclei in the chamber was 51.8 as calculated from the partial pressures.

A comparison between total cross sections is not possible, however, because many single prong oxygen tracks were obviously missed, either because they were too short or because they were confused with helium.* But the inelastic cross sections can still be composed if a value for σ_i/σ_t for oxygen can be found. A recent tabulation on neutron cross sections(16) indicates that for elements in the region of oxygen σ_i/σ_t for 90 Mev neutrons is around 0.38. Because oxygen has an alpha particle structure and in view of the approximate nature of the calculation, σ_i/σ_t is assumed to be the same for oxygen as found for helium in this experiment -- namely 0.49 ± 0.07. Then the expected ratio of inelastic helium events to inelastic oxygen events is

$$\frac{51.8 \times 1.9 \times 10^{-25}\text{cm}^2}{7.65 \times 10^{-25}\text{cm}^2} = 12.9$$

The oxygen cross section was taken from reference (11). The observed ratio is 489/40 = 12.2, which would be smaller if the excited states of oxygen contributed appreciably to the inelastic cross section.

9. Azimuthal Symmetry Check

Since there is no reason to believe otherwise, all processes in this experiment are expected to occur with azimuthal symmetry. Because this has been one of the assumptions employed in this experiment, and in order to be certain that no systematic errors have been made in the angular measurements, one should like to verify this.

The following table shows the number of He^4 recoils, and tritons from pt events, as observed in four azimuthal angle groups.

---

* Many with respect to single prong oxygen -- few with respect to single prong helium.

	0 - 30°	150 - 180°	180 - 210°	330 - 360°
He^4's	93.0 ± 11	73.6 ± 10	75.6 ± 10	81.7 ± 10
Protons from pt	46.3 ± 7	30.4 ± 6	35.7 ± 6	34.6 ± 6

The uncertainties are probable errors based on the number of events actually observed.

VI. CONCLUSIONS

When helium is bombarded by 90 Mev neutrons, the dominant process is elastic scattering, which exhibits the characteristic forward diffraction peak for incident neutron energies above 40 Mev. For neutron energies below 40 Mev elastic scattering tends to become more isotropic. The most frequent inelastic process is the disintegration in which the incident neutron strips off a proton from the helium nucleus leaving a low energy triton behind. A special case of this process occurs when the outgoing neutron and proton proceed together as a high energy forward deuteron -- the so-called pick-up process. Pick-up accounts for about one-half of the events in which a deuteron and a triton are emitted; in the other half the deuteron comes off in a random direction with low energy. Although Heidmann's theory may be criticized in a number of ways, as pointed out by the author, it is in good agreement with the cross sections for elastic scattering and pt and dt disintegrations. The most serious discrepancies arise when the theoretical ratio of forward pick-up deuterons to backward deuterons of 1000/1 is compared with the experimental ratio of 1/1; also the theory predicts a much smaller number of pd and dd disintegration than is observed. As far as the energy dependences are concerned, no marked dependence is evident over the region investigated for

elastic scattering and for pt and pd disintegrations, while the dt disintegrations fall off with increasing energy, as is expected at least for the pick-up part of the process. Noteworthy in the angular distributions is the fact that the proton angular distributions from pt and pd disintegrations reflect to some extent the free n-p interaction. Since He^3's could not be distinguished from He^4's in this investigation, the mechanism leading to He^3 production has been assumed to be similar to that leading to triton production. The possible errors arising from this assumption would seriously affect only the $He^4(n, 2n)He^3$ cross section.

Since at higher incident neutron energies, say 270 Mev, the theoretical approximation that the bombarding particle interacts only with one nucleon in the target nucleus becomes much better, the calculations become simplified, and hence neutron-helium scattering at this energy should prove to be of decisive interest. Further, the parallel experiment to the present one, namely proton-helium scattering at high energies would, together with the results of the present investigation, provide further comparison between the n-n and n-p and p-p forces.

VII. ACKNOWLEDGMENTS

The author wishes to express his sincere gratitude to Professor Wilson Powell for suggesting this problem and for his helpful advice and constant encouragement throughout the investigation. The cooperation of many members of the cloud chamber group is also acknowledged with pleasure, and special thanks are due to Dorothy Gardner for carrying out a large share of the tedious calculations and to

Beverly Lee who did the computation in the earlier stages. The author has profited greatly from discussions of the theoretical aspects with Peter Wolff.

FIGURE CAPTIONS

Fig. 1 Sketch of the cyclotron, cloud chamber and collimation arrangement.

Fig. 2 Photograph of Cloud Chamber, magnet and timing circuits. The neutron beam emerges through the hole in the cement block and enters the cloud chamber on the far side of the magnet platform.

Fig. 3 Sketch of stereoscopic project used for life-size reproduction of tracks.

Fig. 4 Regions of blindness due to limitation on dip angle α. Regions inside the oval are excluded when α is limited to the range from $+30^{\circ}$ to -30°.

Fig. 5 Incident neutron energy distribution as measured from He^4 recoils.

Fig. 6 Incident neutron energy distribution as measured from various inelastic events.

Fig. 7 Angular distribution of elastically scattered neutrons from incident neutrons > 40 Mev.

Fig. 8 Angular distribution of elastically scattered neutrons from incident neutrons < 40 Mev.

Fig. 9 Angular distribution of deuterons from deuteron-triton events.

Fig. 10 Energy distribution of deuterons from deuteron-triton events.

Fig. 11 Energy distribution of tritons from pt events.

Fig. 12 Angular distribution of tritons from pt events.

Fig. 13 Energy distribution of protons from pt events.

Fig. 14 Angular distributions of protons from pt and pd events.

Fig. 15 Energy distribution of protons from pd events.

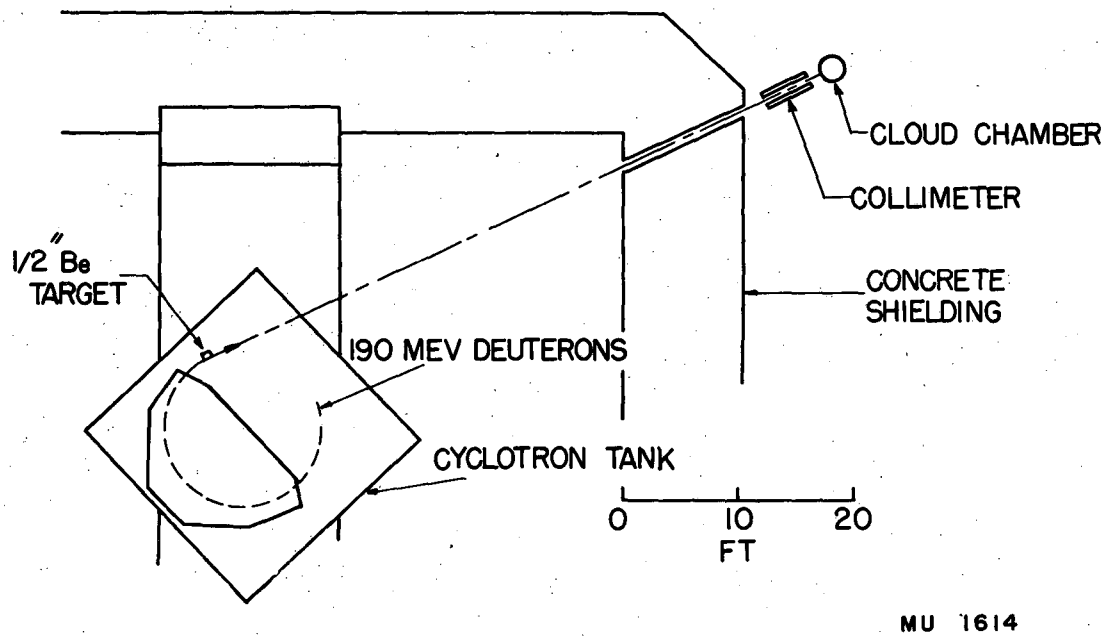
CLOUD CHAMBER
COLLIMETER
1/2" Be
TARGET
CONCRETE
SHIELDING
190 MEV DEUTERONS
CYCLOTRON TANK
0
10
20
FT
MU 1614

Fig. 1

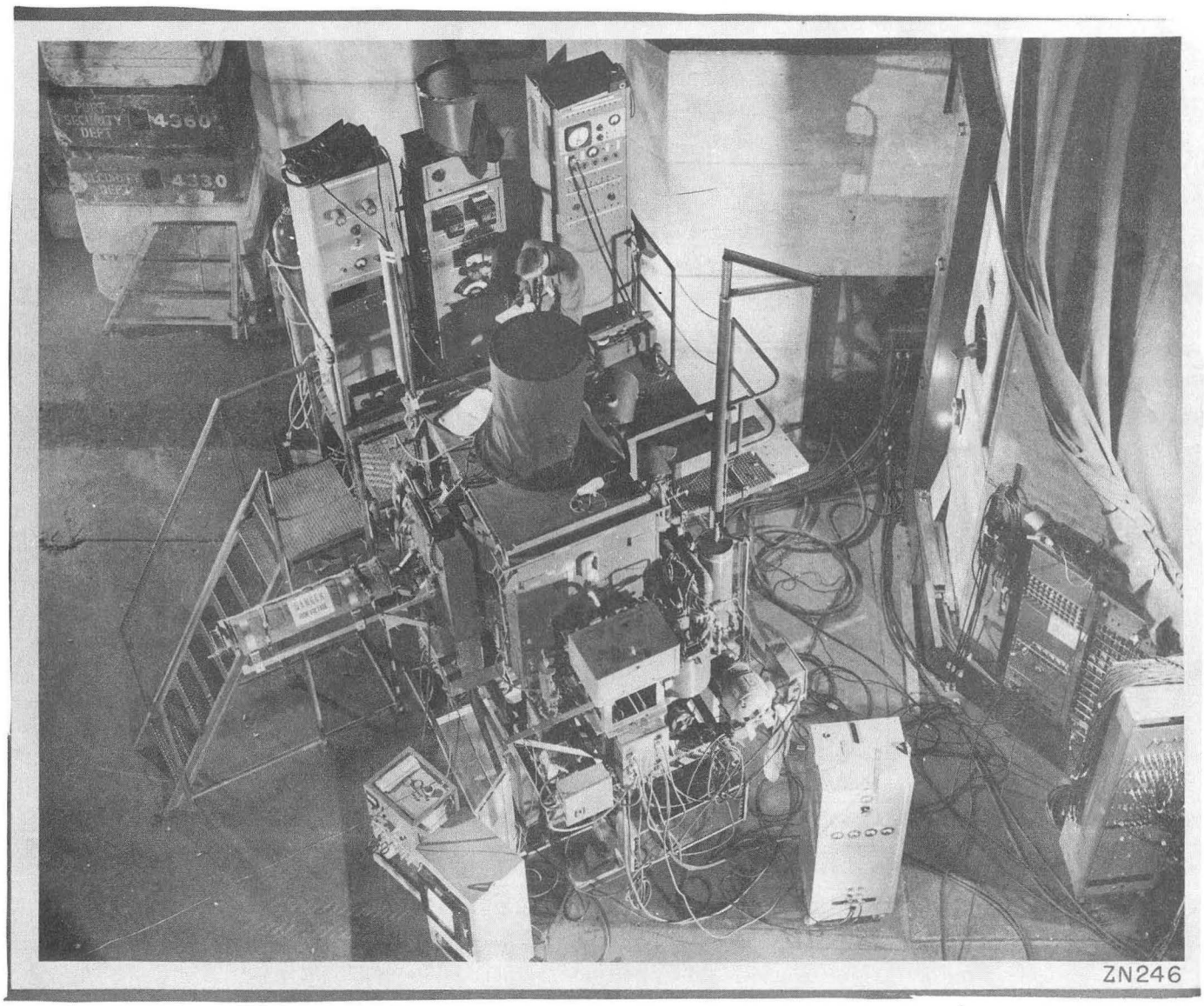

Fig. 2

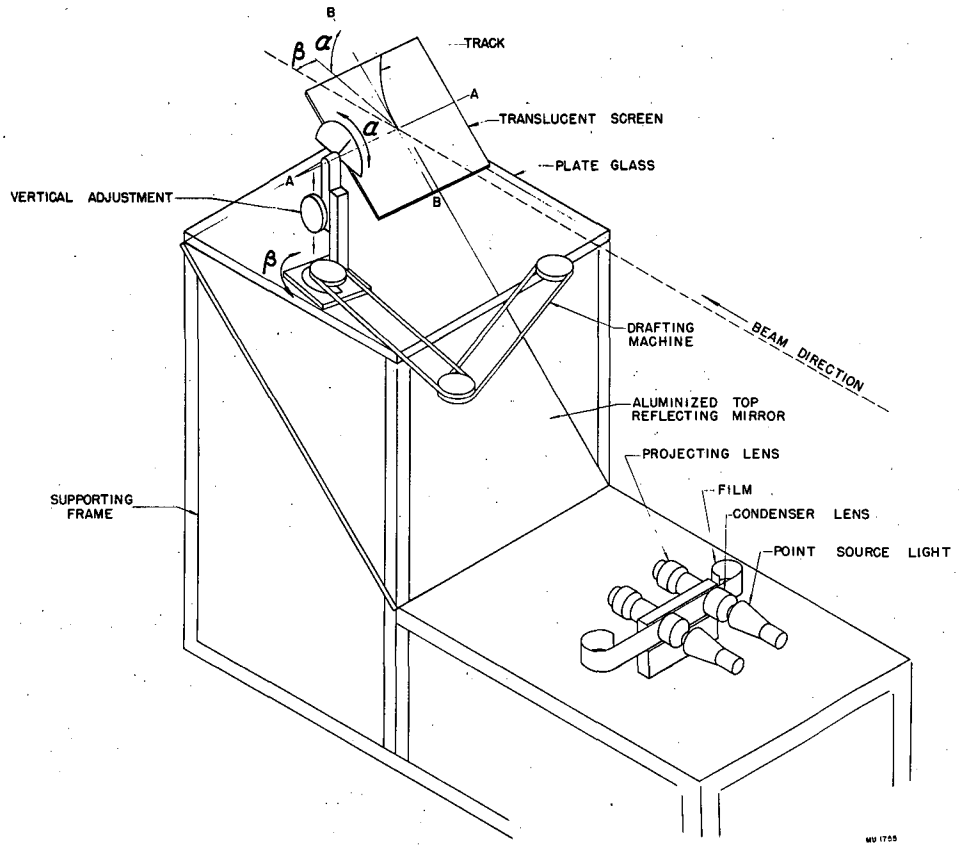
B
β
α
TRACK
A
TRANSLUCENT SCREEN
α
PLATE GLASS
A
VERTICAL ADJUSTMENT
B
β
DRAFTING MACHINE
BEAM DIRECTION
ALUMINIZED TOP REFLECTING MIRROR
PROJECTING LENS
FILM
SUPPORTING FRAME
CONDENSER LENS
POINT SOURCE LIGHT
MU 1755

Fig. 3

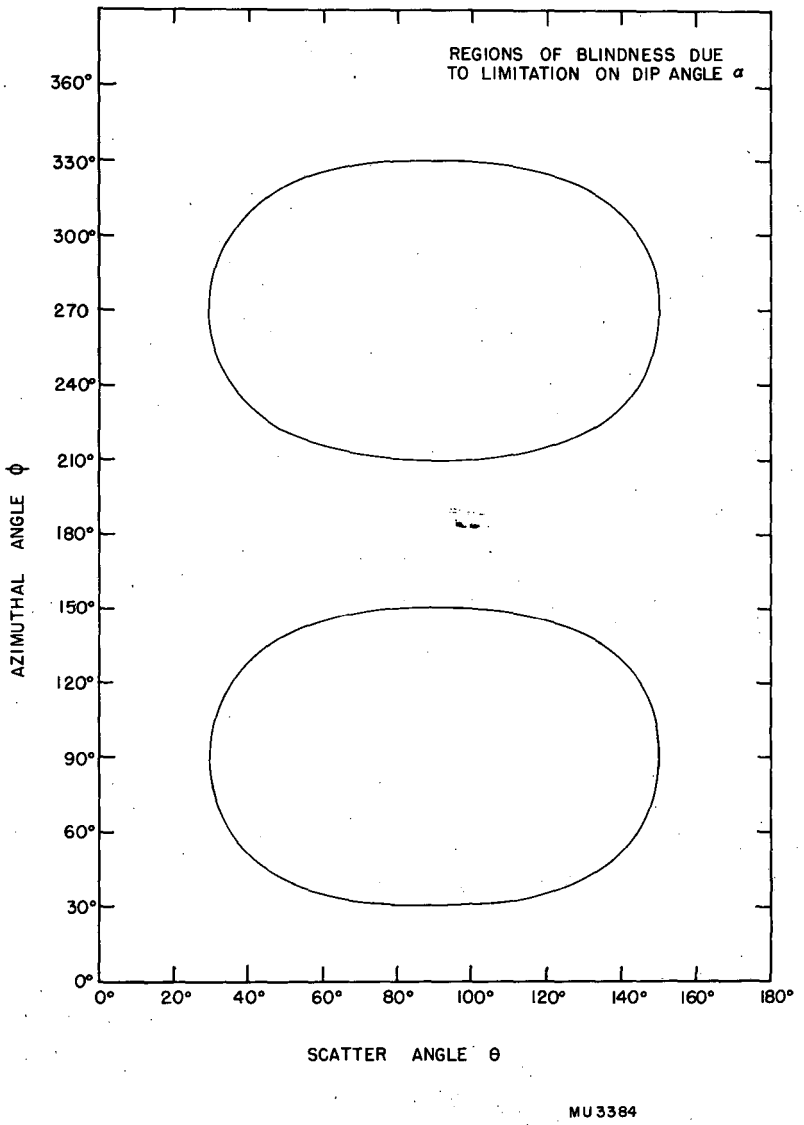
REGIONS OF BLINDNESS DUE
TO LIMITATION ON DIP ANGLE α
360°
330°
300°
270
240°
210°
180°
150°
120°
90°
60°
30°
0°
AZIMUTHAL ANGLE φ
0°
20°
40°
60°
80°
100°
120°
140°
160°
180°
SCATTER ANGLE θ
MU3384

Fig. 4

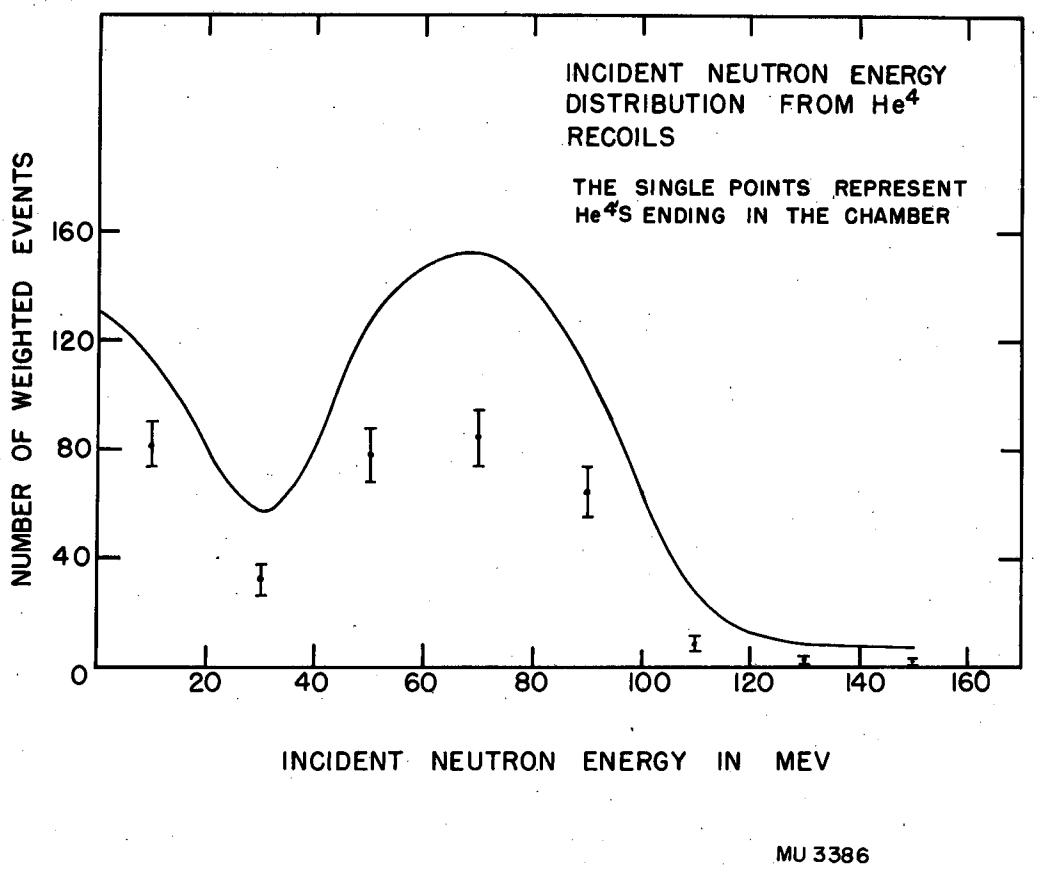
INCIDENT NEUTRON ENERGY DISTRIBUTION FROM He4 RECOILS
THE SINGLE POINTS REPRESENT He4'S ENDING IN THE CHAMBER
NUMBER OF WEIGHTED EVENTS
0
40
80
120
160
20
40
60
80
100
120
140
160
INCIDENT NEUTRON ENERGY IN MEV
MU 3386

Fig. 5

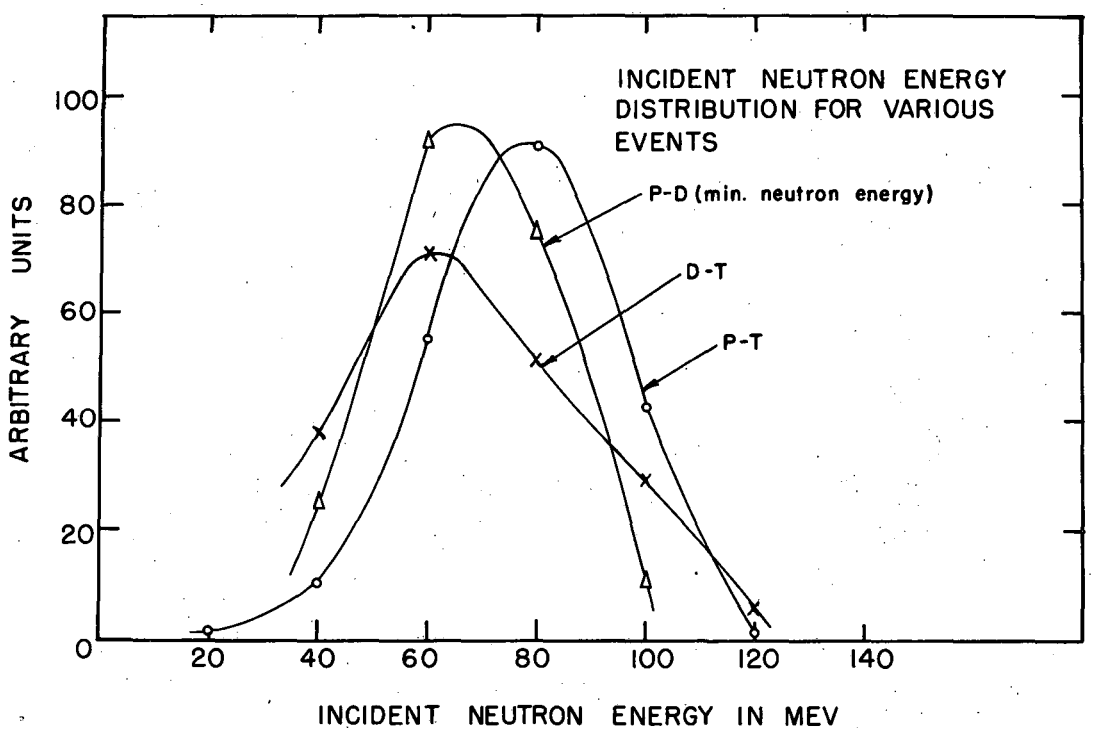
INCIDENT NEUTRON ENERGY DISTRIBUTION FOR VARIOUS EVENTS
P-D (min. neutron energy)
D-T
P-T
ARBITRARY UNITS
0
20
40
60
80
100
20
40
60
80
100
120
140
INCIDENT NEUTRON ENERGY IN MEV

MU 3385

Fig. 6

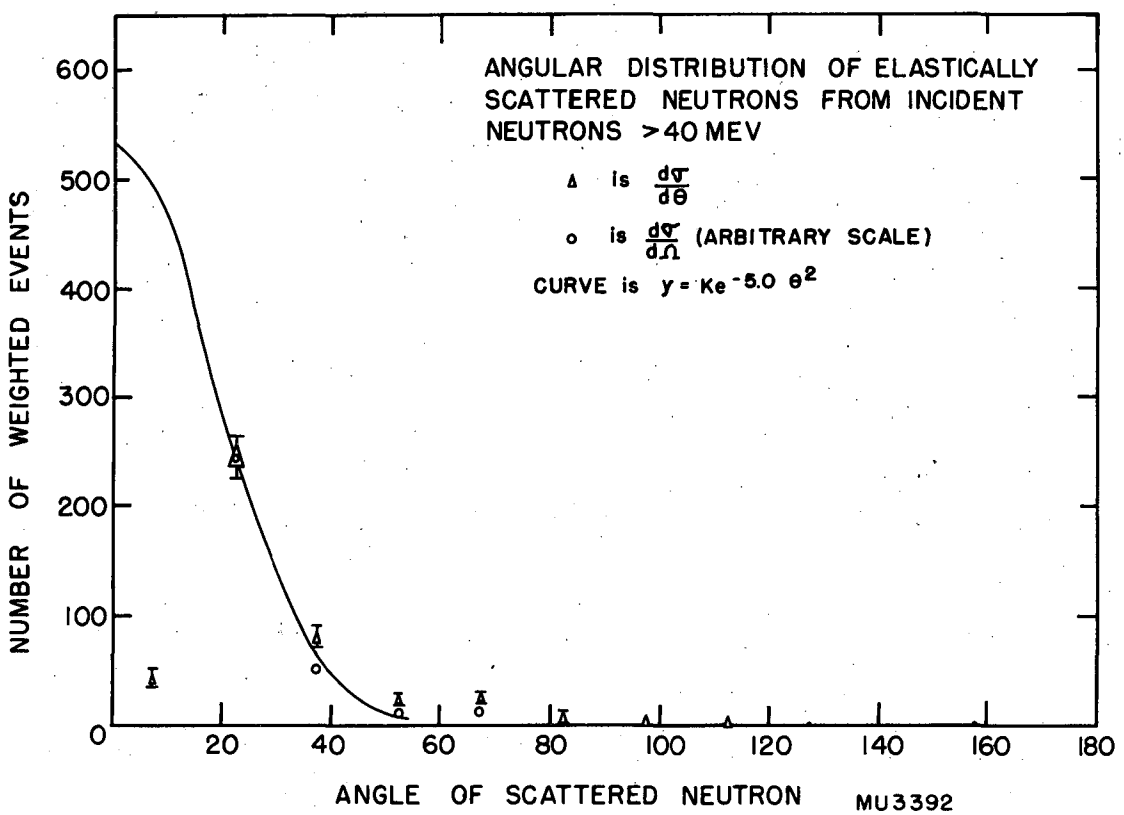
ANGULAR DISTRIBUTION OF ELASTICALLY SCATTERED NEUTRONS FROM INCIDENT NEUTRONS >40 MEV
Δ is dσ/dθ
o is dσ/dΩ (ARBITRARY SCALE)
CURVE is y = Ke^-5.0 θ^2
NUMBER OF WEIGHTED EVENTS
0
100
200
300
400
500
600
20
40
60
80
100
120
140
160
180
ANGLE OF SCATTERED NEUTRON
MU3392

Fig. 7

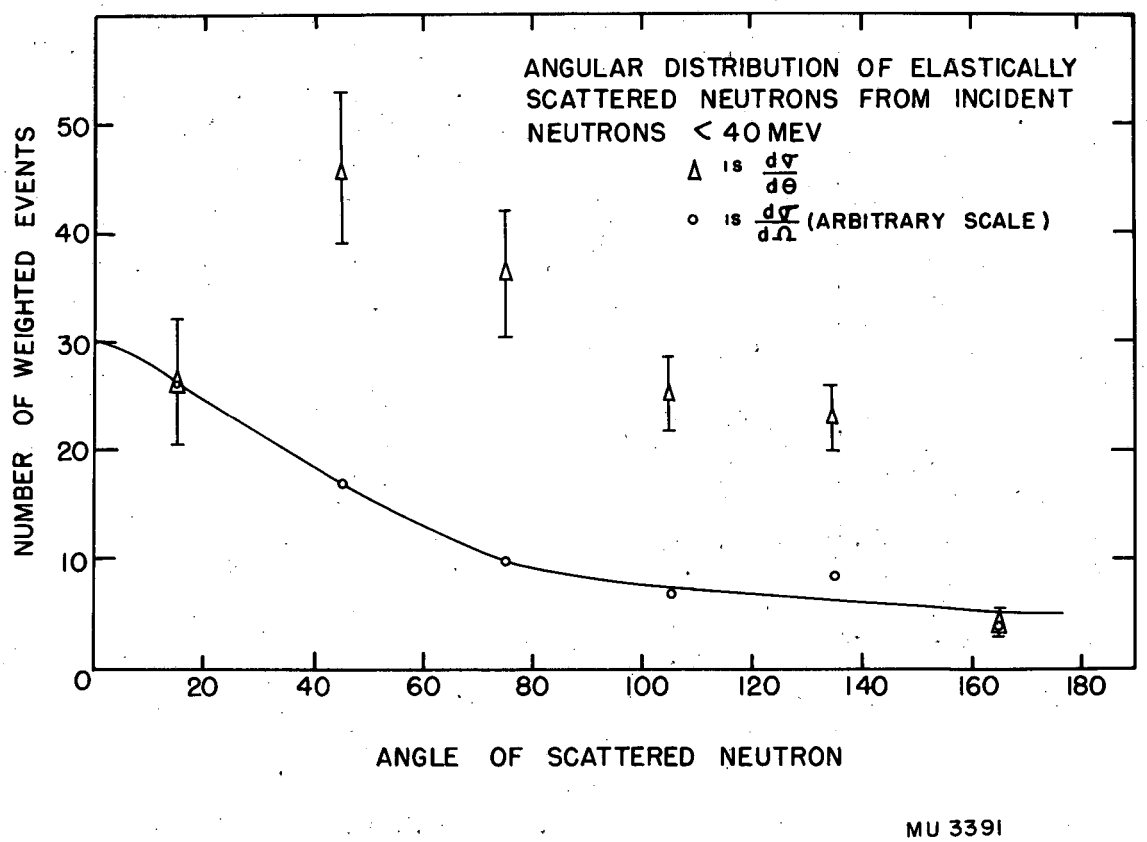
ANGULAR DISTRIBUTION OF ELASTICALLY SCATTERED NEUTRONS FROM INCIDENT NEUTRONS < 40 MEV
Δ IS dσ/dθ
o IS dσ/dΩ (ARBITRARY SCALE)
NUMBER OF WEIGHTED EVENTS
0
10
20
30
40
50
20
40
60
80
100
120
140
160
180
ANGLE OF SCATTERED NEUTRON
MU 3391

Fig. 8

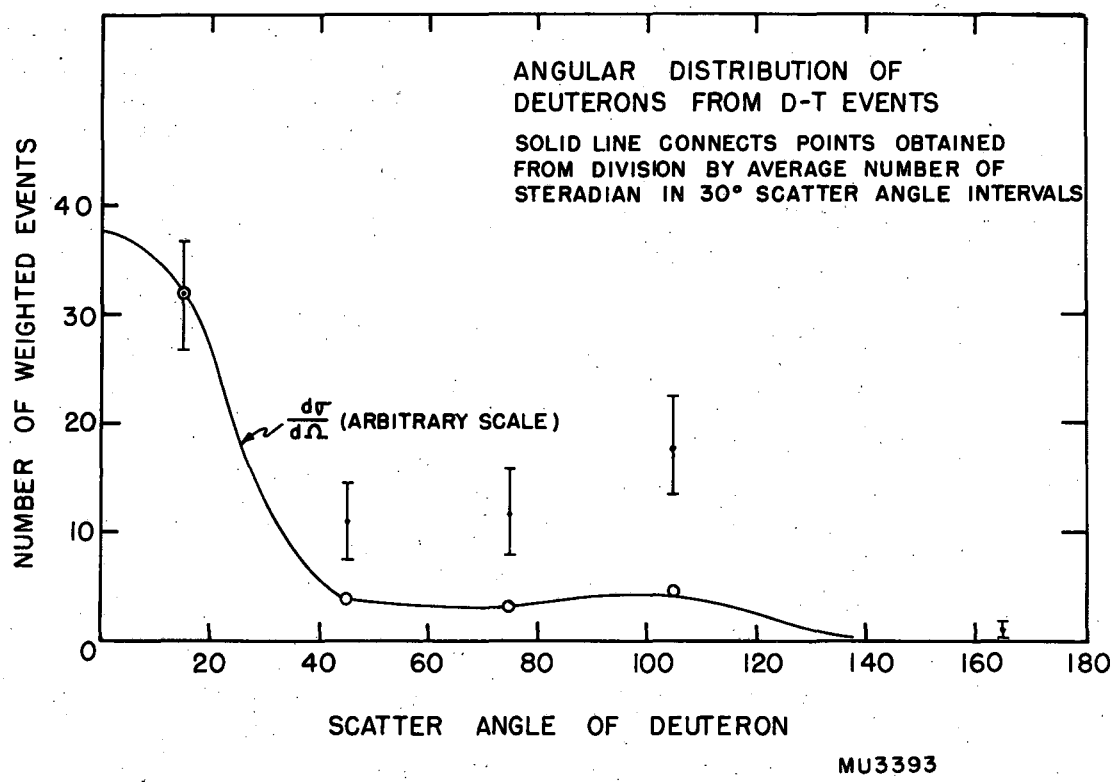
ANGULAR DISTRIBUTION OF
DEUTERONS FROM D-T EVENTS
SOLID LINE CONNECTS POINTS OBTAINED
FROM DIVISION BY AVERAGE NUMBER OF
STERADIAN IN 30° SCATTER ANGLE INTERVALS
NUMBER OF WEIGHTED EVENTS
0
10
20
30
40
$\frac{d\sigma}{d\Omega}$ (ARBITRARY SCALE)
20
40
60
80
100
120
140
160
180
SCATTER ANGLE OF DEUTERON
MU3393

Fig. 9

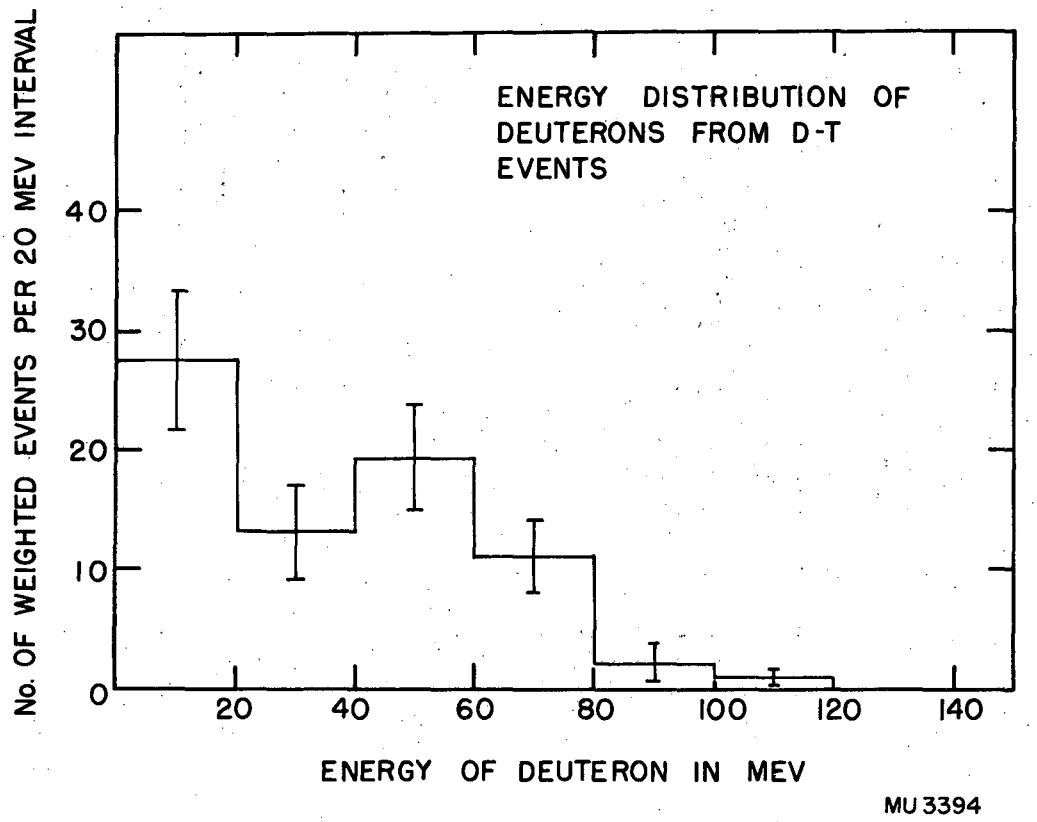
ENERGY DISTRIBUTION OF DEUTERONS FROM D-T EVENTS
No. OF WEIGHTED EVENTS PER 20 MEV INTERVAL
0
10
20
30
40
20
40
60
80
100
120
140
ENERGY OF DEUTERON IN MEV
MU 3394

Fig. 10

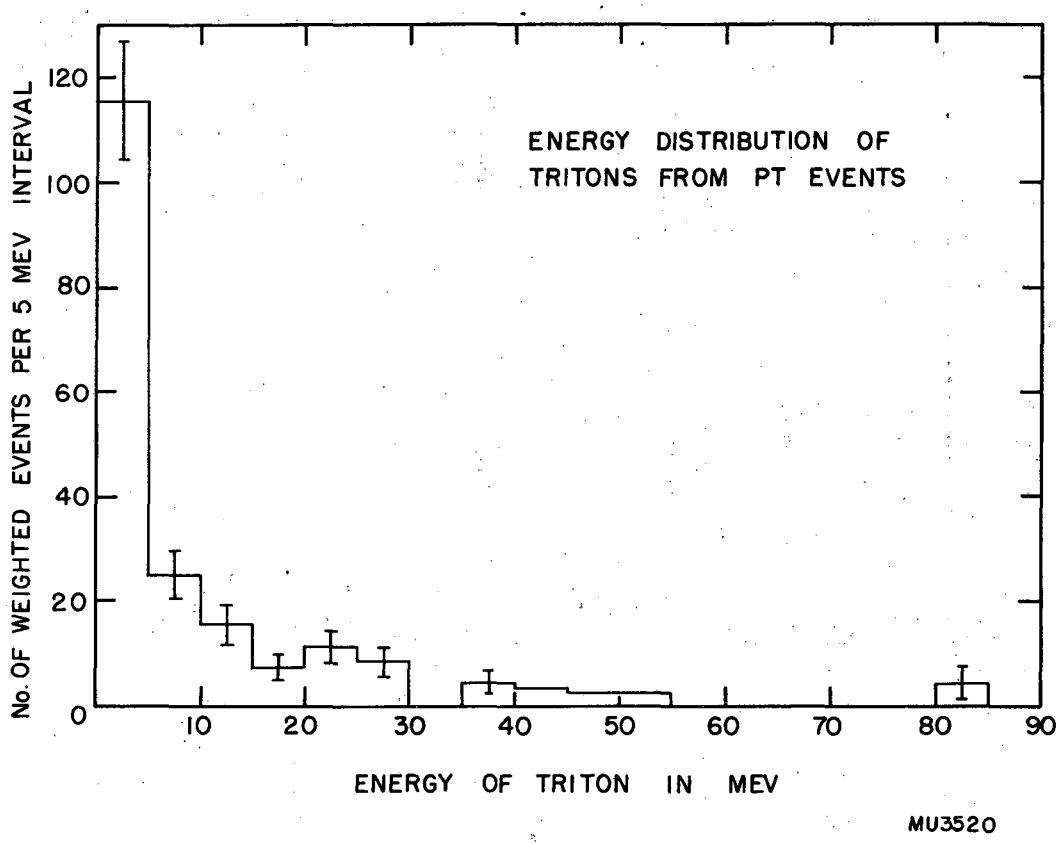
ENERGY DISTRIBUTION OF
TRITONS FROM PT EVENTS
No. OF WEIGHTED EVENTS PER 5 MEV INTERVAL
0
20
40
60
80
100
120
10
20
30
40
50
60
70
80
90
ENERGY OF TRITON IN MEV
MU3520

Fig. 11

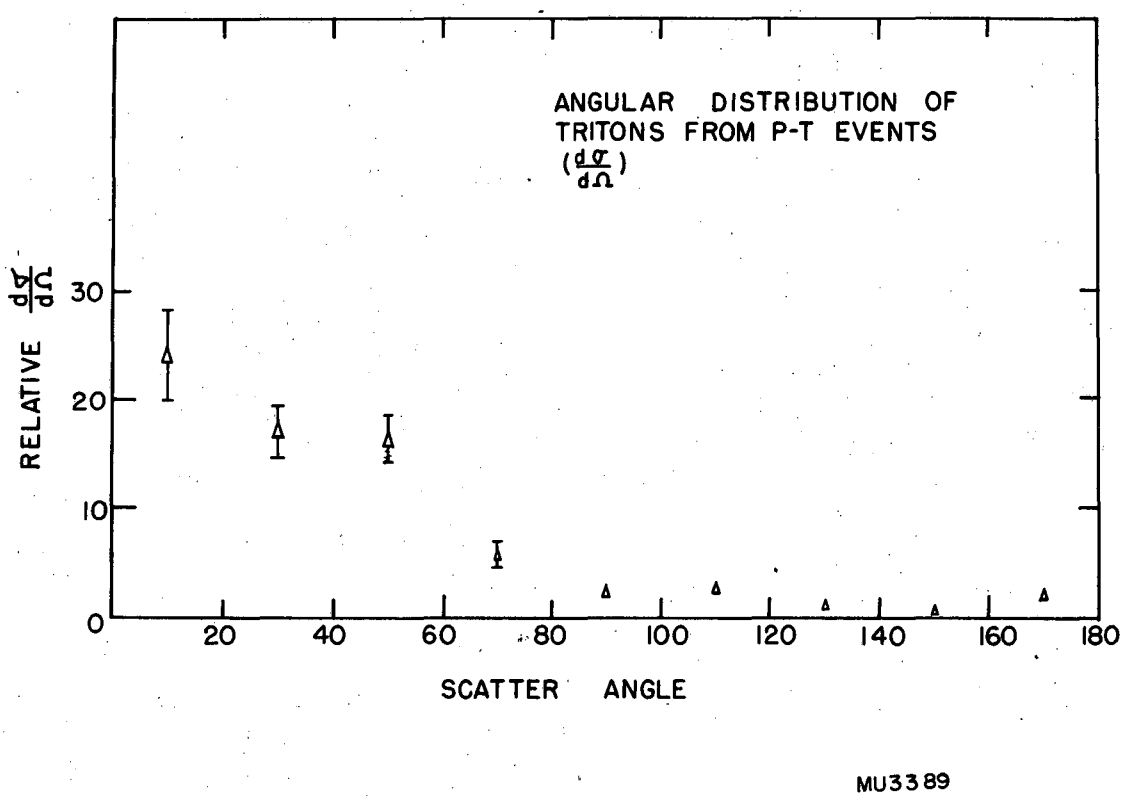
ANGULAR DISTRIBUTION OF
TRITONS FROM P-T EVENTS
$(\frac{d\sigma}{d\Omega})$
RELATIVE $\frac{d\sigma}{d\Omega}$
30
20
10
0
20
40
60
80
100
120
140
160
180
SCATTER ANGLE
MU3389

Fig. 12

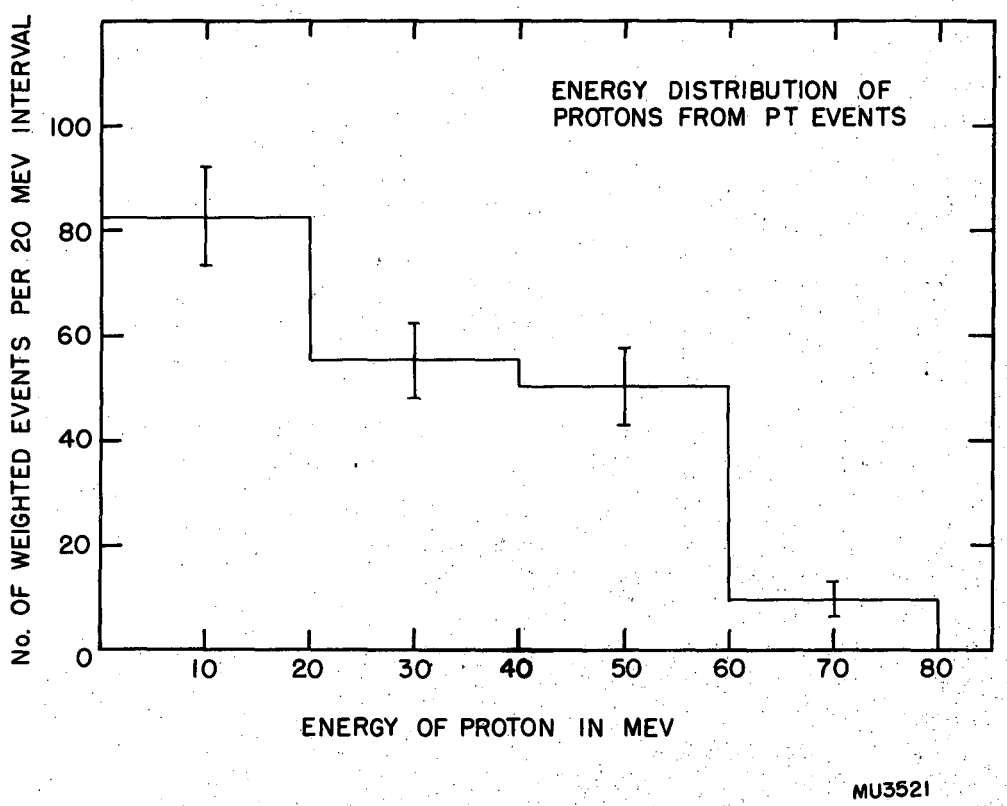
ENERGY DISTRIBUTION OF
PROTONS FROM PT EVENTS
No. OF WEIGHTED EVENTS PER 20 MEV INTERVAL
0
20
40
60
80
100
10
20
30
40
50
60
70
80
ENERGY OF PROTON IN MEV
MU3521

Fig. 13

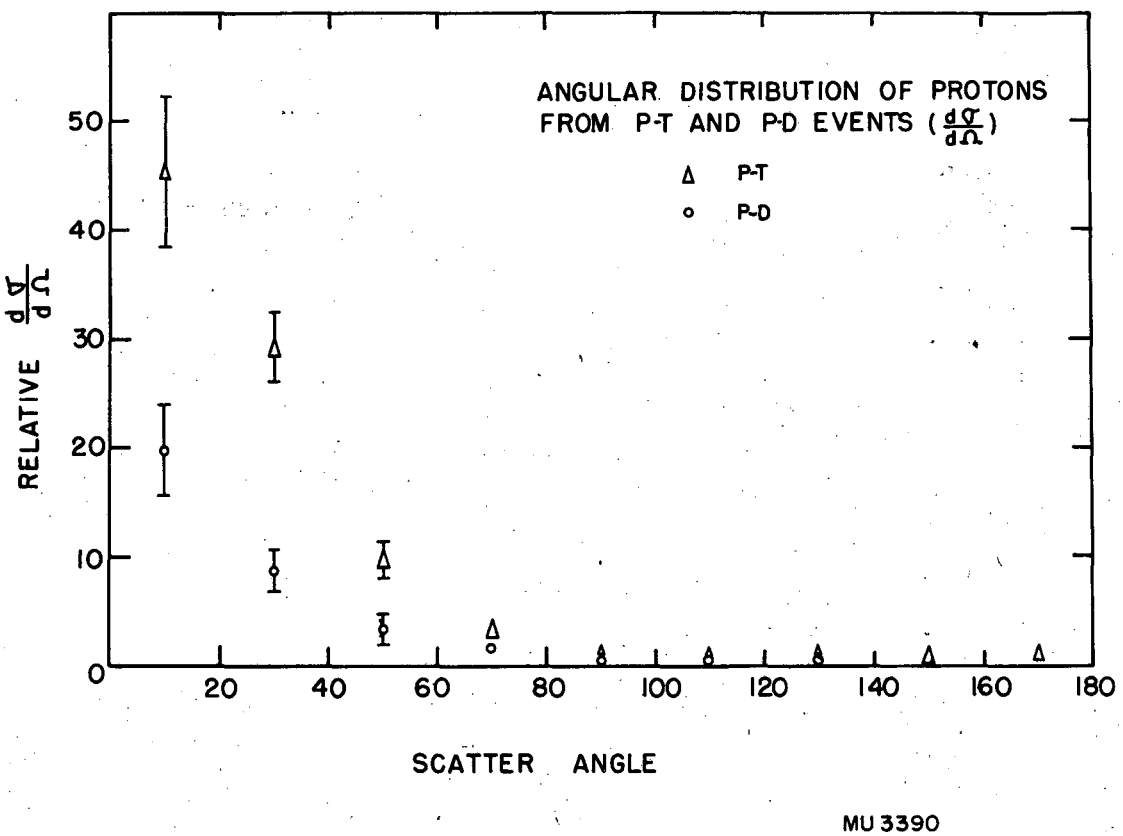
ANGULAR DISTRIBUTION OF PROTONS
FROM P-T AND P-D EVENTS ($\frac{d\sigma}{d\Omega}$)
Δ P-T
o P-D
RELATIVE $\frac{d\sigma}{d\Omega}$
0
10
20
30
40
50
20
40
60
80
100
120
140
160
180
SCATTER ANGLE
MU 3390

Fig. 14

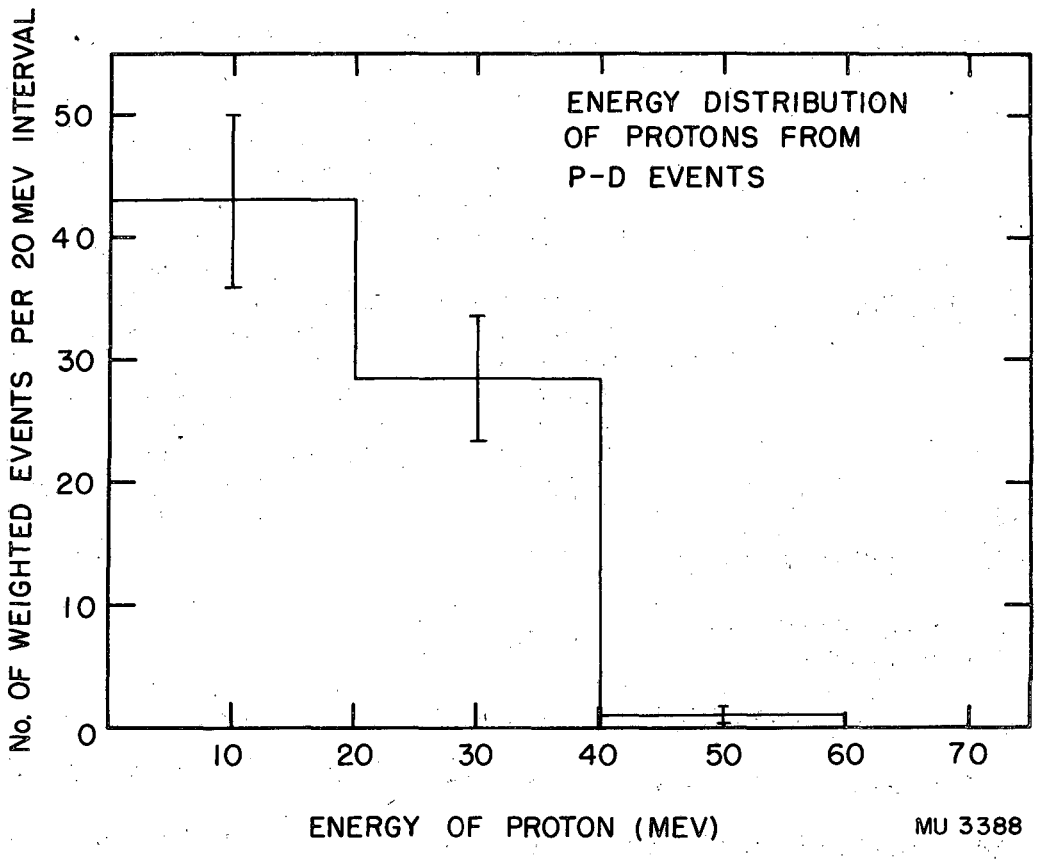
ENERGY DISTRIBUTION
OF PROTONS FROM
P-D EVENTS
No. OF WEIGHTED EVENTS PER 20 MEV INTERVAL
0
10
20
30
40
50
10
20
30
40
50
60
70
ENERGY OF PROTON (MEV)
MU 3388

Fig. 15

APPENDIX I. DEFINITIONS

Dip angle α	The angle between the initial direction of the track and the horizontal plane containing the neutron beam, measured in a vertical plane.
Beam angle β	The angle between the projection of the initial track direction on the horizontal plane and the direction of the neutron beam, measured in a horizontal plane.
Scatter angle θ	The angle between the initial track direction and the neutron beam.
Azimuthal angle ϕ	The angle between the projection of the initial track direction on a plane perpendicular to the neutron beam and the horizontal plane.
Slant radius ρ_s	The radius of curvature measured in the plane of the track.
Radius ρ	$\rho = \rho_s \cos\alpha$, and is the radius of curvature which a particle of slant radius ρ_s would have if it were moving in a plane perpendicular to the magnetic field with the same momentum.
Slant plane	Is the plane containing the initial track direction and the horizontal line perpendicular to the initial track direction. It is approximately the plane of the track except that in general the path of a charged particle in a magnetic field describes a helix. The slant plane is at dip angle α to the horizontal plane.
Transverse Momentum	$H\rho_t = H\rho \sin\theta$
Momentum in the beam direction	$H\rho_z = H\rho \cos\theta$

APPENDIX II. SAMPLE ANALYSIS OF TWO PICTURES

The following pictures serve as examples of the type of events that were analyzed. The letters are abbreviations for the particles and the numbers stand for the dE/dx values with respect to minimum ionization. The lightest tracks which were dealt with were about 4-5 times with respect to minimum and are probably not visible in the reproduction; the heaviest tracks encountered were sometimes

as high as 400 times with respect to minimum. The vertical line through the center of each picture is ruled on the chamber top glass and indicates the direction of the neutron beam. The equally spaced horizontal reference markings intersecting the vertical line are used for stereo-lining up of the pictures.

Fig. A is interesting in that it shows, among other things, the characteristic endings of several different particles. The spiral path of the proton ending is clearly evident in the right half of the picture. The two tritons originating from the two helium stars between the first and second reference mark near the vertical center line both end in the chamber. The He^4 recoil just above the lowest reference mark ends in the chamber and is typically near 90° to the beam. The longest prong from the 4-prong oxygen star near the center of the picture looks like an alpha particle ending. (No analysis of oxygen stars was made).

Fig. B includes one of the two He^3's identified in this experiment which ends in the chamber. Its characteristic ending can be compared with the He^4 ending just above the 4th reference mark. Both pictures show a number of other helium disintegrations.

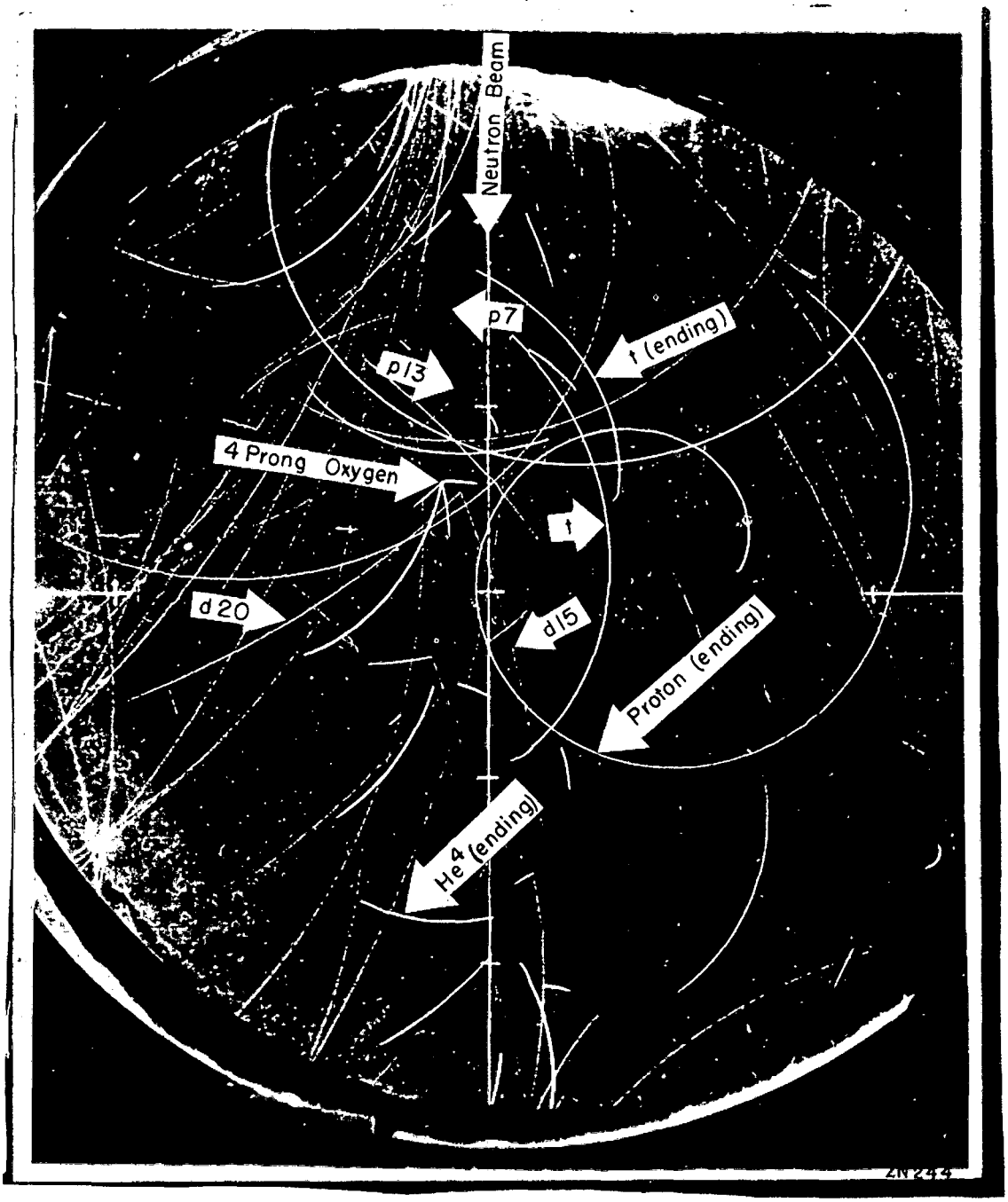
Neutron Beam
p7
t (ending)
p13
4 Prong Oxygen
t
d20
d15
Proton (ending)
He 4 (ending)

Fig. A

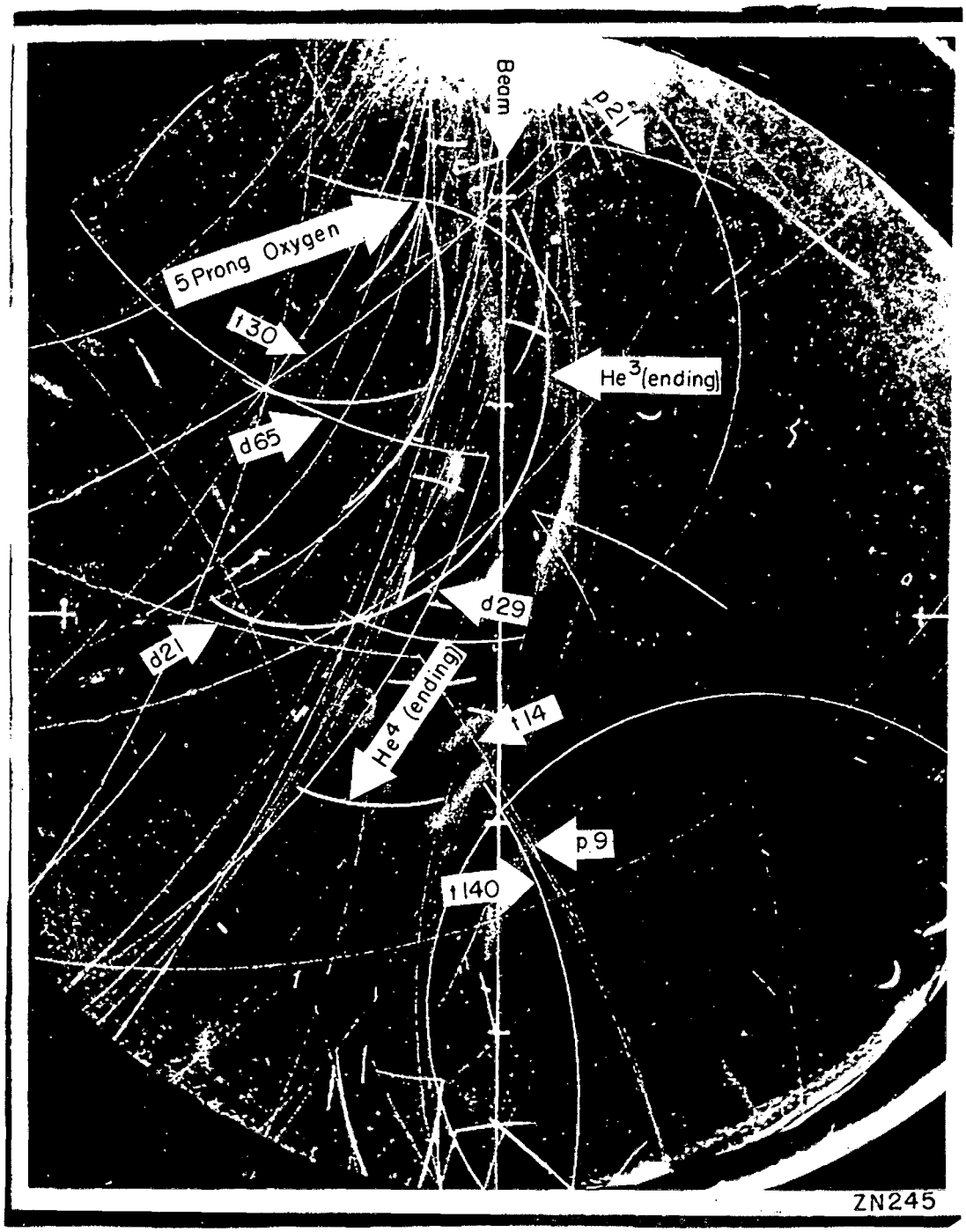
Beam
p21
5 Prong Oxygen
t30
He3 (ending)
d65
d29
d21
He4 (ending)
t14
p9
t140
ZN245

Fig. B

APPENDIX III. DERIVATION OF FORMULAS

1. PT and DD Cases

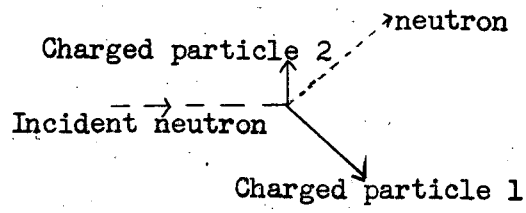

In both cases one neutron is ejected in the disintegration. The following equations apply:

$$E_n = E_1 + E_2 + B.E. + E_{n'}$$

$$E_{n'} = \frac{p^2_{n'}}{2m} = \frac{p^2_{n't} + p^2_{n'z}}{2m}$$

$$E_n = \frac{p^2_{nz}}{2m} = \frac{(p_{1z} + p_{2z} + p_{n'z})^2}{2m}$$

$$p_{n't} = p_{1t} + p_{2t}$$

where E_n, p_n = energy and momentum of incident neutron

E_1, E_2 = energies of ejected charged particles

B.E. = binding energies of the particles (or threshold of the reaction)

$E_{n'}$, $P_{n'}$ = energy and momentum of ejected neutron

t = transverse component of momenta

z = momenta components along beam direction

prime = ejected neutron

Algebraic manipulation of the equations leads to

$$p_{n'z} = \frac{E_1 + E_2 + B.E. + p^2_{n't} \times K - (p_{1z} + p_{2z})^2 \times K}{2(p_{1z} + p_{2z}) \times \sqrt{K}},$$

where K is the appropriate factor to convert the units. Hence $E_{n'}$ and E_n can be obtained immediately.

2. DT Case

This is the two-body problem, and E_n can be computed in two ways.

$$E_n = E_1 + E_2 + B.E.$$

$$E_n = \frac{p_{nz}^2}{2m} = \frac{(p_{1z} + p_{2z})^2}{2m}$$

3. PD Case

The best that can be done here is to lump the two ejected neutrons into one particle of 2 neutron masses; then the energy associated with the momentum of the 2 neutrons will always be a minimum. Thus

$$E_n = E_1 + E_2 + B.E. + E'_{min}.$$

$$E'_{min} = \frac{p_{n'}^2}{2 \times 2m} = \frac{p_{n't}^2 + p_{n'z}^2}{2 \times 2m}$$

$$E_n = \frac{p_{nz}^2}{2m} = \frac{(p_{1z} + p_{2z} + p_{n'z})^2}{2m}$$

After algebraic manipulation these equations lead to

$$p_{n1_z} = -2(p_{1z} + p_{2z}) \sqrt{K} \pm \sqrt{2(p_{1z} + p_{2z})^2 \times K + 2(E_1 + E_2 + B.E.) + p_{n't}^2 \times K}$$

4. Binding Energies

Process	B.E.
dt	17.6 Mev
pt	19.8
dd	23.8
pd	25.9
pp	28.1
He^3	20.5

APPENDIX IV. ENERGY AND IONIZATION OF LIGHT PARTICLES AS A FUNCTION OF $H\rho$

ρ	$H\rho$	P		D		H^3		He^3		He^4	
cm.	gauss cm.	E	$\frac{dE}{dx}$ *	E	$\frac{dE}{dx}$ *	E	$\frac{dE}{dx}$ *	E	$\frac{dE}{dx}$ *	E	$\frac{dE}{dx}$ *
1	21,700	.03		.02		.01		.04		.03	
1.5	32,550	.04		.02		.01		.05		.04	
2	43,400	.09		.04		.03		.12		.09	
2.5	54,250	.10		.05		.03		.13		.10	
3	65,100	.20	351	.10		.07		.27		.20	
3.5	75,950	.30	298	.15		.10		.40		.30	
4	86,800	.40	259	.20		.13		.50		.40	
4.5	97,650	.50	226	.25		.17		.70		.50	
5	108,500	.60	202	.28		.20		.80		.60	
5.5	119,350	.70	180	.35		.23		.90		.70	
6	130,200	.80	160	.40	343	.27		1.1		.80	
6.5	141,050	1.0	146	.50	321	.33		1.3		1.0	
7	151,900	1.1	140	.55	296	.37		1.5		1.1	
7.5	162,750	1.3	128	.65	271	.43		1.7		1.3	
8	173,600	1.4	122	.74	257	.47		1.9		1.4	
8.5	184,450	1.6	110	.82	228	.53	347	2.1		1.6	
9	195,300	1.8	98	.92	224	.60	336	2.4		1.8	
9.5	206,150	2.0	86	1.0	208	.67	320	2.7		2.0	
10	217,000	2.3	78.5	1.1	198	.76	300	3.1	580	2.3	
10.5	227,850	2.5	73.5	1.3	187	.83	284	3.3	560	2.5	
11	238,700	2.7	68.5	1.4	178	.91	275	3.6	539	2.7	
11.5	249,550	3.0	61.0	1.5	165	1.0	258	4.0	510	3.0	
12	260,400	3.2	58.8	1.6	158	1.1	247	4.3	488	3.2	
12.5	271,250	3.5	55.5	1.8	147	1.2	233	4.7	456	3.5	
13	282,100	3.8	52.2	1.9	146	1.3	227	5.1	424	3.8	584
13.5	292,950	4.1	49.1	2.1	142	1.4	218	5.5	392	4.1	572
14	303,800	4.4	46.6	2.2	140	1.5	211	5.9	368	4.4	560
14.5	314,650	4.7	44.0	2.4	132	1.6	204	6.3	344	4.7	539
15	325,500	5.1	40.8	2.5	128	1.7	193	6.8	314	5.1	512
15.5	336,350	5.4	39.1	2.7	125	1.8	189	7.2	302	5.4	500
16	347,200	5.7	37.3	2.9	122	1.9	182	7.6	289	5.7	488
16.5	358,050	6.1	35.2	3.1	116	2.1	173	8.1	274	6.1	464
17	368,900	6.5	33.5	3.3	110	2.2	169	8.7	259	6.5	440
17.5	379,750	6.9	31.8	3.5	104	2.3	162	9.2	247	6.9	416
18	390,600	7.3	30.4	3.7	98	2.4	156	9.7	235	7.3	392
18.5	401,450	7.7	29.2	3.9	92	2.6	151	10.3	225	7.7	368
19	412,300	8.1	27.9	4.1	86	2.7	147	10.8	217	8.1	344
19.5	423,150	8.5	26.9	4.3	82.3	2.9	146	11.3	209	8.5	331
20	434,000	9.0	25.5	4.5	78.5	3.0	145	12.0	200	9.0	314
20.5	444,850	9.4	24.7	4.8	75.5	3.2	142	12.5	194	9.4	305
21	455,700	9.9	23.6	5.0	73.5	3.3	140	13.2	186	9.9	294
21.5	466,550	10.4	22.7	5.2	71.5	3.5	135	13.9	178	10.4	284
22	477,400	10.9	21.9	5.5	68.5	3.6	133	14.5	171	10.9	274
22.5	488,250	11.4	21.1	5.7	65.5	3.8	128	15.2	163	11.4	259

MU 3469

ρ	$H\rho$	P		D		H^3		He^3		He^4	
cm.	gauss cm.	E	$\frac{dE}{dx}$*	E	$\frac{dE}{dx}$*	E	$\frac{dE}{dx}$*	E	$\frac{dE}{dx}$*	E	$\frac{dE}{dx}$*
23	499,100	11.9	20.4	6.0	61.0	4.0	126	15.9	158	11.9	244
23.5	509,950	12.4	19.7	6.2	60.1	4.1	125	16.5	154	12.4	240
24	520,800	12.9	19.0	6.5	58.8	4.4	122	17.2	149	12.9	235
24.5	531,650	13.4	18.4	6.8	56.8	4.6	117	17.9	144	13.4	229
25	542,500	14.0	17.8	7.0	55.5	4.7	115	18.7	139	14.0	222
25.5	553,300	14.6	17.2	7.3	53.8	4.9	110	19.5	134	14.6	215
26	564,200	15.1	16.7	7.7	52.2	5.1	116	20.1	131	15.1	209
26.5	575,050	15.7	16.1	8.0	50.5	5.3	102	20.9	126	15.7	203
27	585,900	16.3	15.7	8.2	49.1	5.5	98	21.7	122	16.3	196
27.5	596,750	16.9	15.2	8.5	47.9	5.7	94	22.5	119	16.9	191
28	607,600	17.5	14.8	8.8	46.6	5.9	90	23.3	115	17.5	186
28.5	618,450	18.1	14.4	9.2	45.1	6.1	86	24.1	112	18.1	181
29	629,300	18.8	13.9	9.5	44.0	6.4	82.7	25.1	108	18.8	176
29.5	640,150	19.5	13.5	9.8	42.4	6.6	80.6	26.0	105	19.5	169
30	651,000	20.1	13.2	10.1	40.8	6.8	78.5	26.8	102	20.1	163
31	672,700	21.5	12.5	10.7	39.1	7.2	75.5	28.7	97.1	21.5	156
32	694,400	22.8	12.0	11.5	37.3	7.6	72.4	30.4	92.7	22.8	149
33	716,110	24.3	11.3	12.2	35.2	8.1	68.5	32.4	87.6	24.3	141
34	737,800	25.5	10.9	12.9	33.5	8.7	65.1	34.0	84.7	25.5	134
35	759,500	27.1	10.4	13.8	31.8	9.2	62.2	36.1	80.8	27.1	127
36	781,200	29.0	9.8	14.6	30.4	9.8	58.8	38.7	76.0	29.0	122
37	802,900	30.6	9.3	15.5	29.2	10.4	56.5	40.8	72.9	30.6	117
38	824,600	32.0	9.0	16.5	27.9	11.0	54.1	42.7	70.1	32.0	112
39	846,300	33.7	8.6	17.3	26.9	11.5	52.2	44.9	66.8	33.7	108
40	868,000	35.4	8.3	18.0	25.5	12.0	50.7	47.2	64.1	35.4	102
41	889,700	37.0	8.0	19.0	24.7	12.7	48.5	49.3	61.7	37.0	99
42	911,400	38.6	7.7	19.9	23.6	13.3	46.6	51.5	59.2	38.6	94
43	933,100	40.7	7.4	20.8	22.7	13.9	44.9	54.2	56.8	40.7	91
44	954,800	42.2	7.2	21.8	21.9	14.6	42.8	56.3	55.0	42.2	88
45	976,500	44.1	6.9	22.7	21.1	15.3	40.8	58.8	52.8	44.1	84
46	998,200	46.5	6.6	23.9	20.4	15.9	39.7	62.0	50.9	46.5	82
47	1,019,600	48.1	6.5	25.0	19.7	16.6	38.5	64.1	49.6	48.1	79
48	1,041,600	50.0	6.2	26.0	19.0	17.3	37.3	66.7	48.0	50.0	76
49	1,063,300	52.0	6.1	26.9	18.4	18.0	36.2	69.4	46.5	52.0	74
50	1,085,000	54.8	5.8	28.0	17.8	18.8	35.0	73.1	44.5	54.8	71
51	1,106,700	56.1	5.7	29.4	17.2	19.8	33.5	74.8	43.6	56.1	69
52	1,128,400	58.2	5.5	30.5	16.7	20.6	32.3	77.6	42.2	58.2	67
53	1,150,100	60.3	5.4	31.7	16.1	21.2	31.5	80.4	40.8	60.3	64
54	1,171,800	62.6	5.2	32.8	15.7	22.0	30.4	83.5	39.2	62.6	63
55	1,193,500	65.0	5.1	34.0	15.2	22.9	29.6	86.7	38.2	65.0	61
56	1,215,200	67.5	4.9	35.0	14.8	23.5	29.1	90.0	37.1	67.5	59
57	1,236,900	70.2	4.8	36.3	14.4	24.8	27.9	93.6	36.0	70.2	58
58	1,258,600	72.2	4.7	37.5	13.9	25.6	27.1	96.3	35.3	72.2	56
59	1,280,300	74.5	4.6	38.8	13.5	26.3	26.3	99.3	34.5	74.5	54
60	1,302,000	78.0	4.4	40.3	13.2	27.0	25.5	104	33.2	78.0	53

MU3470

ρ	$H\rho$	P		D		H^3		He^3		He^4	
cm.	gauss cm.	E	$\frac{dE}{dx}$ *	E	$\frac{dE}{dx}$ *	E	$\frac{dE}{dx}$ *	E	$\frac{dE}{dx}$ *	E	$\frac{dE}{dx}$ *
61	1,323,700	80.8	4.3	41.5	12.8	28.0	24.9	108	32.0	80.8	51
62	1,345,400	82.3	4.2	42.6	12.5	29.0	24.2	110	31.4	82.3	50
63	1,367,100	84.0	4.2	43.9	12.3	29.9	23.6	112	30.8	84.0	49
64	1,388,800	87.3	4.0	45.5	12.0	30.8	23.1	116	30.2	87.3	48
65	1,410,500	89.7	3.9	47.0	11.6	31.9	22.5	120	29.6	89.7	47
66	1,432,200	93.8	3.8	48.5	11.3	32.9	21.9	125	28.8	93.8	45
67	1,453,900	95.5	3.8	50.0	11.1	34.0	21.4	127	28.4	95.5	44
68	1,475,600	98.1	3.7	51.3	10.9	35.0	20.9	131	27.5	98.1	44
69	1,497,300	102	3.6	52.8	10.7	36.0	20.4	136	26.4	102	43
70	1,519,000	105	3.5	54.5	10.4	36.9	20.3	140	26.0	105	42
71	1,540,700	107	3.5	56.3	10.1	38.0	20.0	143	25.6	107	41
73	1,584,100	112	3.4	59.0	9.7	40.0	19.4	149	25.0	112	39
76	1,649,200	122	3.2	63.8	9.0	43.3	18.5	163	23.5	122	
80	1,736,000	135	2.9	70.8	8.3	47.8	17.2	180	21.6	135	
84	1,822,800	149	2.7	78.0	7.7	52.5	15.9	199	19.6	149	
88	1,909,600	161	2.6	85.4	7.2	58.1	14.3	215	18.4	161	
93	2,018,100	178	2.4	95.2	6.7	64.4	12.5	237	16.8	178	
98	2,126,600	198	2.3	105	6.1	70.6	11.7	264		198	
103	2,235,100	215	2.1	116	5.7	78.8	10.7	287		215	
108	2,343,600	235	2.0	127	5.2	85.8	9.8	313		235	
113	2,452,100	254	1.9	140		94.7	9.3	339		254	
119	2,582,300	280	1.8	153		104	8.8	373		280	
125	2,712,500	303	1.7	169		115	8.2	404		303	
131	2,842,700	333	1.7	186		126	7.6	444		333	
137	2,972,900	356	1.6	201		138	6.9	475		356	
144	3,124,800	388	1.5	223		151	6.2	517		388	
151	3,276,700	420	1.5	244		167	5.9	560		420	
158	3,428,600	454	1.4	268		183	5.5	606		454	
166	3,602,200	492	1.4	289		200	5.1	656		492	
174	3,775,800	532	1.3	318		220	4.7	709		532	
182	3,949,400	572	1.3	344		239		763		572	
191	4,144,700	619	1.2	374		262		825		619	

MU3471

The energy values are generally accurate to 5 percent, except in the low energy region, and except for He^3 and He^4 for which a non-relativistic conversion was made.

The dE/dx values were obtained for protons in helium from the Aron(1) tables except below 1 Mev. The rest of the dE/dx columns were obtained by approximate non-relativistic proportionalities and interpolation over wide ranges. Therefore no greater accuracy than 15 percent can be assigned to them.

---

* The dE/dx values are relative to Minimum ionization.

(1) Aron, Hoffman, and Williams, Range-Energy Curves AECU-663 UCRL-121

REFERENCES

1. K. Brueckner and W. Powell, P.R. 75 1274 (1949)
2. J. Hadley and H. J. York, P.R. 80 345 (1950)
3. M. Goldberger, P.R. 74 1269 (1948)
4. G. Chew and M. Goldberger, P.R. 77 470 (1950)
5. J. Tracy and W. Powell, P.R. 77 594 (1950)
6. W. Powell, Rev. Sci. Instr. 20 402 (1949)
7. W. Powell, "Scattering of High Energy Deuterons by 90 Mev Neutrons", P.R. in print. See also UCRL-1191
8. Brueckner, Hartsough, Hayward and Powell, P.R. 75 555 (1949)
9. J. Tracy, M. S. Thesis, 1949, Dept. of Electrical Engineering, University of California
10. Estimated from Hadley, Kelley, Leith, Segré, Wiegand and York, P.R. 75 351 (1949) and Chamberlain, Segré and Wiegand, P.R. 83 923 (1951)
11. Cook, McMillan, Peterson and Sewell, P.R. 75 7 (1949)
12. J. Heidmann, Phil. Mag. 41 444 (1950)
13. J. Heidmann, private communication
14. A. Bratenahl, private communication
15. C. Swartz, P.R. 85 73 (1952)
16. Summary of Neutron Cross Section Measurements for 14 Mev to 280 Mev Neutrons; Hildebrand, Hicks and Harker, UCRL-1305 6 (1951)